The Luminosity Oscillations Imager, a space instrument: from design to science

By THIERRY APPOURCHAUX

European Space Agency, Advanced Concept and Science Payloads Office,
P.O.Box 299, 2200AG Noordwijk, The Netherlands
Present address: Institut d'Astrophysique Spatiale, Université Paris XI - C.N.R.S,
Bâtiment 121, 91405 Orsay Cedex, France

The Luminosity Oscillations Imager (LOI) is a part of the VIRGO instrument aboard the Solar and Heliospheric Observatory (SOHO) launched on December 2, 1995. The main scientific objectives of the instrument were to detect solar g and p modes in intensity. The instrument is very simple. It consists of a telescope making an image of the Sun onto a silicon detector. This detector resolves the solar disk into 12 spatial elements allowing the detection of degree lower than 7. The guiding is provided by 2 piezoelectric actuators that keep the Sun centred on the detector to better than 0.1". The LOI serves here as an example for understanding the logical steps required for building a space instrument. The steps encompasses the initial scientific objectives, the conceptual design, the detailed design, the testing, the operations and the fulfillment of the initial scientific objectives. Each step is described in details for the LOI. The in-flight and ground-based performances, and the scientific achievements of the LOI are mentioned. When the loop is looped, it can assessed whether a Next Generation LOI could be useful. This short course can serve as a guide when one wishes to propose a space instrument for a new space mission.

---

1. Introduction

The building of a space instrument is not a simple affair. In order to justify the building of a space instrument, one should demonstrate that there is a definite needs implying that the scientific objectives cannot be achieved from the ground. It is sometimes easier to justify to go to space when light from specific spectral region (EUV, UV) does not reach the ground. In the case of an optical instrument, other arguments are required for going to space. For instance the absence of atmosphere can considerably improve image quality for there is no seeing in space. With the advent of adaptative optics, a large range of space mission may not be required anymore. Nevertheless, the stability and homogeneity of the images obtained from space cannot be matched by those of the ground. In recent years with the flourishing of helio- and asteroseismology, other needs related to the measurement of light intensity fluctuations became a sound justification for going to space.

In this lecture, I would like to guide the reader in all the steps, (or in as many as I can), that are necessary for achieving Science with a space instrument. For that end, I will take as an example the instrument I built for the Solar and Heliospheric Observatory: the Luminosity Oscillations Imager.

2. From science to instrument building

The design and building phase of any instrument can be summarized by Fig. 1. There are two distinct phases: the design and the building of the instrument. The first phase includes the following steps:

(a) Scientific objectives
(b) Scientific requirements

(*c*) Implementation of requirements
(*d*) Technical requirements
(*e*) Instrument design

Step (a) defines what kind of science one wishes to achieve. Step (b) defines what kind of observables is needed in order to fulfill Step (a). The observables can be images in selected wavelength, spectrum analysis in any wavelength, polarimetry, particle distribution, it can be any information carried out by photons or any other particles (protons, neutrons, electrons, neutrino). Step (c) defines the concept of the instrument that will return the observables. It is not yet a detailed instrument design but more a conceptual approach on the instrument: spectrograph, narrow band spectrum analyzer, polarimeter, particle counter, imager. Step (d) transforms the concept into an instrument and imposes technical requirements on the instrument such as temperature stability, resolution, field-of-view. At this step this is where one usually performs a trade off analysis between different technical solutions. Finally, Step (e) sets the detailed design of the instrument into an instrument to be assembled. All the technical requirements are then translated into building and interface requirements. The second phase or building phase includes the following steps:

(*a*) Instrument building
(*b*) Integration
(*c*) Testing
(*d*) Operations
(*e*) Achievements of the objectives: Science

Step (a) sets the building requirements and the interface requirements between the different part to be assembled. These can be mechanical, electrical or thermal interfaces. Step (b) is the integration of the building block of the instrument that should fit together given the interface requirements. Step (c) is the test of the whole instrument or part of the instrument. The testing of the parts can be done before integration. The testing also involves calibration of the instrument and environmental testing if required. Finally, Step (d) is the successful operation of the instrument that will provide in the end the Science in Step (e). This last step can then be compared with the initial scientific objectives set before building the instrument. The achievements (or lack of) will then be used for building the Next Generation of instruments: more demanding and more performing.

3. What is different about a space instrument?

The two phases described above are not necessarily different for a ground or space based instrument. The main difference lies in the boundary and environment conditions that are very different for a space mission compared to a ground-based observatory. The boundary conditions are the following:

(*a*) Mass (kg)
(*b*) Volume (cm^3)
(*c*) Power (Watt)
(*d*) Telemetry (kbps)
(*e*) Long lifetime (years)
(*f*) Money (Euro)

The mass of the instrument is limited by the number of instruments making the payload of the mission and by the capability of the launcher used for putting the spacecraft into space. The volume is limited for it has to fit somehow inside the fairing of the launcher. The power is also limited by the number of instruments and by the size of the solar array. The telemetry rate, the amount of data to be transmitted to the ground, is also limited

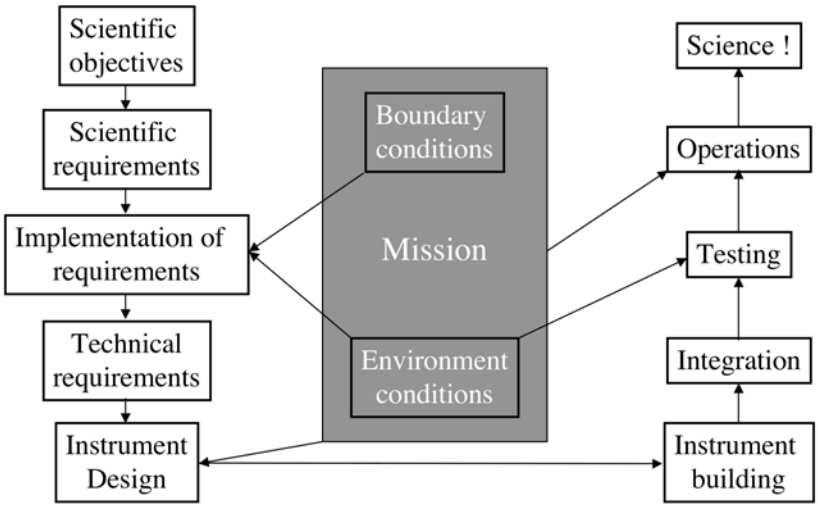

FIGURE 1. The burden of the instrumentalist: from concept to building. The flow chart on the left hand side summarizes the conceptual phase of the design of the instrument. The flow chart of the right hand side summarizes the building phase of the instrument. The difference between a ground based and a space based instrument is exemplified by the grey box in the middle. The boundary conditions are different.

by the number of instruments, by the power of the transponder, by the distance of the spacecraft to the ground and by the size of the receiving antenna. Last but not least, although it is commonly admitted that space instrumentation is more expensive than ground-based instrumentation, it is nevertheless required to build the instrument within a limited budget. The higher cost is related to the fact that repair is not an option in space† and that high reliability parts should be used; this will ensure a long lifetime. All these boundary conditions are taken into account during the implementation of the requirements and at all latter steps till the instrument design.

The environment conditions are the following:

(a) Launch loads
(b) Thermal interfaces and vacuum
(c) Electromagnetic interfaces
(d) Energetic particles
(e) Solar irradiations (or from other bodies)

During the launch, random vibrations created by a combination of acoustic noise and structural deformations are going to impact onto the physical integrity of the instrument. Random loads can be up to 20 g. If care is not taken about internal resonance in the instrument, it is likely that much higher load of about 100-200 g are likely to break critical part of the instrument. When in space, the instrument has to establish a thermal equilibrium that is achieved by radiative and conductive exchange; there is no more luxury for convection cooling in vacuum. Electromagnetic emission and compatibility should ensure that electric noise will be set to a minimum. This point can be very critical to instruments measuring electric or magnetic fields in space. Energetic particles

† The Hubble Space Telescope was made repairable and upgradable but it should not be formally ranked as a space instrument

(protons, electrons, heavy ions) will affect the functioning of analog an digital electronics by creating performance degradation or even transient disruption (Single Event Upset or Latch ups). Finally, solar irradiations (or from other bodies) will radiatively heat the instrument but will also affect the optical properties of glass materials and thermal coatings. These environment conditions set the scene for the testing phase that will be significantly different from that of a ground-based instrument. The following tests have to be performed:

- Vibrations (Step a)
- Thermal vacuum (Step b)
- EMC/EMI (Step c)
- Irradiations (Step d and e)
- Thermal balance (Step e)

When the first four steps are passed with success, i.e. the instrument performs nominally after these stringent tests, the instrument is then so-called space qualified. It means that the instrument should nominally operate during the mission. The last test is usually not performed at the instrument level but when the overall spacecraft is built. It consists in simulating the illumination of the Sun in a realistic thermal environment in vacuum.

The building of a space instrument requires more attention than any other type of instrument. The amount of product assurance (i.e. paper work) is such that each single change needs to be recorded, documented and approved. This additional work (or burden) is an insurance that everything that needs to be known about the instrument can be latter used in case of malfunction during the mission. This is the only way that the instrument can be *repaired* in flight.

4. The Luminosity Oscillations Imager

4.1. *Scientific objectives*

In the mid-80's, helioseismology was emerging as a powerful tool to infer the internal structure of the Sun. The observations of many eigenmodes of the Sun was starting to enable inferences about the internal structure of the Sun. The Tenerife conference held in Puerto de la Cruz in September 1988 was a major milestone for helioseismic research (ESA SP-286). This conference provides a proper snapshot of the knowledge derived from helioseismology at the times. This conference was held right after the selection of the payload for the Solar and Heliospheric Observatory (SOHO) mission. At the times only the p modes had been detected. The p modes were observed in solar radial velocity with amplitude of about a few cm/s and periods of about 5 minutes. The p modes propagate from the visible surface down to 0.2 $R_\odot$ enabling to infer the structure and dynamics of the Sun from the surface to below the convection zone ($r \approx 0.4 R_\odot$). The undetected g modes are confined under the convection zone. From that property, it was clear that the detection of g modes would have considerably improved our knowledge of the structure and dynamics of the solar core. The detection of g modes had been claimed by Delache and Scherrer (1983) but confirmations were still seek by van der Raay (1988) (and references in ESA SP-286). The g-mode detection was one of the main scientific objectives of the helioseismic instruments aboard SOHO. There were three investigations aboard SOHO aiming at detecting the elusive g modes: GOLF (Global Oscillations at Low Frequencies) (Damé, 1988), SOI/MDI (Solar Oscillations Investigation / Michelson Doppler Imager) (Scherrer et al., 1988), VIRGO (Variability of solar IRradiance and Gravity Oscillations) (Fröhlich et al., 1988a). A sub-unit of

VIRGO was specially dedicated to the detection of g modes: the Luminosity Oscillation Imager (LOI).

4.2. *Scientific requirements*

The main scientific requirements of the LOI were the following:

- Detect low-degree oscillations modes (p and g modes at $l < 6$)
- Detection of the modes in intensity fluctuations
- Determine the frequencies, amplitudes for eigenmodes in the frequency range of 1 μHz to 10 mHz.
- Solar noise limited
- Uninterrupted observations

The degree of a mode (l) is one of the quantum number of a spherical harmonics that represents the spatial distribution of the eigenfunctions. At the time, it was thought that only the low degree g modes would have a significant amplitude (Berthomieu and Provost, 1990). In addition, it was believed that the modes needed to be detected not only in solar radial velocities (GOLF, MDI) but also in intensity; the difference in noise generated by convection would help to detect the faint g-mode signals. For instance, the amplitudes to be detected were about a few part-per-million (ppm) for the p modes, and predicted to be about a few tenth of ppm for g modes. Given the mode frequencies, a rather stable instrumentation was required for time period ranging from a few hours to a few minutes. The aim was also to be limited not by the instrumental noise but by the solar noise. At the time, the solar noise had been measured in intensity by ACRIM aboard the Solar Maximum Mission by Woodard (1984) and by the IPHIR instrument aboard Phobos by Fröhlich et al. (1988b) (See Fig 8).

4.3. *Implementation of requirements*

The scientific requirements given above imposed several constraints on the instrument design that is even more severely constrained by the various boundary and environment conditions of the SOHO mission. The implementation of the requirements leads to the following design:

- Low-resolution detector
- Image of the Sun (telescope)
- Internal pointing
- Observe solar continuum avoiding variable Fraünhofer lines
- Stable detector
- Stable acquisition system

The detector should have tens of pixels in order to detect the low degree modes, requiring therefore an imaging capability for the instrument. In order to compensate for likely jittering of the image on the detector due to spacecraft motion and misalignment, an internal pointing system should keep the Sun centered on the detector. The latter should have a quantum efficiency as insensitive as possible to temperature changes. In addition, the acquisition system (analog to digital conversion) should not degrade the performance of the overall instrument. The instrument to be built following these requirements will be subject to several external conditions. The main boundary conditions are the following:

- Mass less than 2.5 kg
- Power less than 2.5 Watt
- Volume: $30 \times 9 \times 9$ cm^3
- Telemetry less than 10 bits/s
- Pointing:
  - Absolute better than 5 arc min

- Short term: relative better than 1 arc sec over 15 min.
- Medium term: relative better than 10 arcsec over 6 months

Some of these conditions are somewhat easy to achieve (telemetry). One should keep in mind that the instrument will be subject of various environmental conditions as given by the Experiment Interface Document Part A (spacecraft requirements also known as the SOHO EID-A). They read as follows:

- Nominal mission lifetime: 2 years
- Orbit: halo orbit around L1 Lagrangian point of the Sun-Earth system
- Dose rate for nominal mission: less than 10 krads behind 2-mm Aluminium shield for a 2-year mission
- Stringent cleanliness requirements
- Launch loads of 12 g's rms all axes.
- Temperature range: 0 to 40 degree C

The lifetime of the mission is set by the cost of operating a spacecraft and by the achievements of the scientific objectives. The orbit chosen for the SOHO here ensures a continuous viewing of the Sun that is so essential for helioseismic investigations. The dose rate is the energy deposited by electrons, protons and heavy ions particles that are likely to damage optics and electronics alike. The cleanliness requirements are imposed by the UV instruments aboard SOHO that are extremely sensitive to any polymerization of hydrocarbon contaminants by the solar UV and blue light (Bonnet et al., 1978). Loads during the launch plays also a major rôle in the design of the instrument. The temperature variations are mainly set by the orbit chosen and by the thermal control performed by the spacecraft.

4.4. *Technical requirements and design*

4.4.1. *General concept*

The design of the LOI instrument was an original idea of Andersen et al. (1988). The instrument concept was to make an image of the Sun onto a low resolution detector, and to detect intensity fluctuations of the surface of the Sun. The instrument as designed and as built was described by Appourchaux et al. (1995a). A cutout of the instrument is shown in Fig. 3 and the conceptual design in Fig. 2. The LOI consists of a telescope imaging the Sun through a narrow passband filter. The image is projected onto a photodiode array detector. The detector is made out of 12 scientific pixels and of 4 guiding pixels. The shape of the scientific pixels is trimmed to detect modes for $l < 7$. The great advantage of this configuration is that we can isolate and identify individual l, m modes for up to $l = 6$ (Appourchaux and Andersen, 1990). The error signals given by the guiding pixels are used to keep the Sun centred on the detector using piezoelectric actuators. The current of each scientific pixel is amplified and digitized using Voltage-to-Frequency Converters (VFCs). The 12 scientific pixels are read simultaneously while the 4 guiding pixels are read sequentially. The sampling time of the instrument is 60 s. The integration time of the scientific pixels is about 99% of the sampling time. Thanks to a sun that never sets on SOHO, the temperature variations of the spacecraft will be minimal. That is why the instrument is not thermally stabilized. It is sometimes better to have open loops than closed loops. I will hereafter describe each main component of the LOI, these are the:

- Telescope
- Entrance filter
- Detector
- Guiding system
- Acquisition system

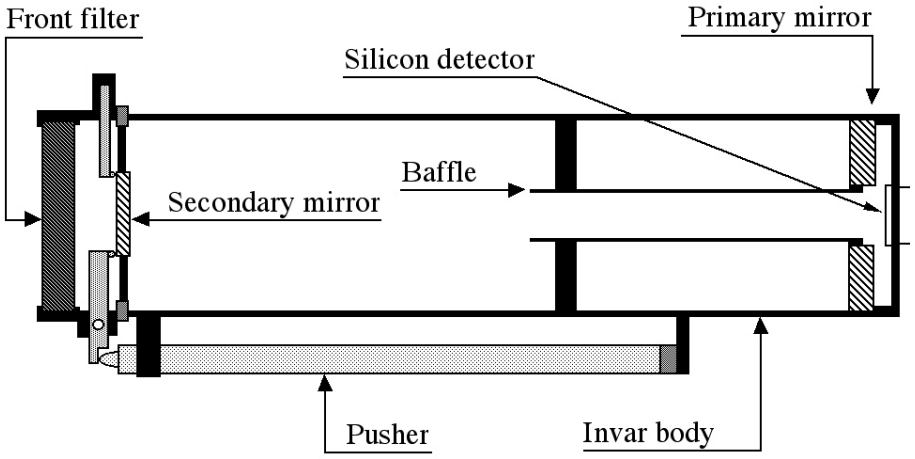

FIGURE 2. Conceptual view of the LOI design. It can be noted that the cylindrical telescope tube is closed by the entrance filter and by the detector. The only openings are the necessary gaps for the lever arm pushing on the secondary mirror mount.

For each the technical requirements and the design is detailed. The interface specifications for each will be quickly explained. These latter specifications are usually very technical and drafted by the engineering team. Nevertheless, these interactions between that team and the instrument scientist is key in developing a sound instrument.

4.4.2. *Telescope: requirements*

The telescope design was driven by the following set of constraints:

- Image size
- Compactness
- Limited aberrations
- Stable focal length
- Pointing needs

The size of the image was driven by the solid state detector. We chose to have a large detector in order to minimize the size of the tracks (See Section 4.5). At the time, in the 90's, a detector based on a silicon wafer of 15 mm square was possible without pushing the technology. The mean solar image size was chosen to be 13-mm diameter. This will set the constraint for the focal length needed for the observations. It should be pointed out that the location of the SOHO spacecraft at L1 is such that the solar angular size is on average 1% larger. The focal length was chosen to be f=1300 mm providing a mean solar angular size of D=12.22 mm. These two numbers will drive the design of the telescope and of the size of the detector.

The compactness of the telescope was an important constraint. The overall instrument including electronics should be fitted in a box 35-cm long by 6-cm square. Given the large focal length and the size of the telescope this imposed to have a 2-mirror telescope with a primary and a secondary mirror.

Like in any optical design, it is crucial to minimize any sort of aberrations. From this point of view, a simple Cassegrain telescope with a parabolic primary mirror and an hyperbolic secondary mirror is not sufficient. The choice was to have a Ritchey-Chrétien with hyperbolic mirrors. This combination has the advantage of minimizing the coma on the edge of the field (Chrétien, 1958).

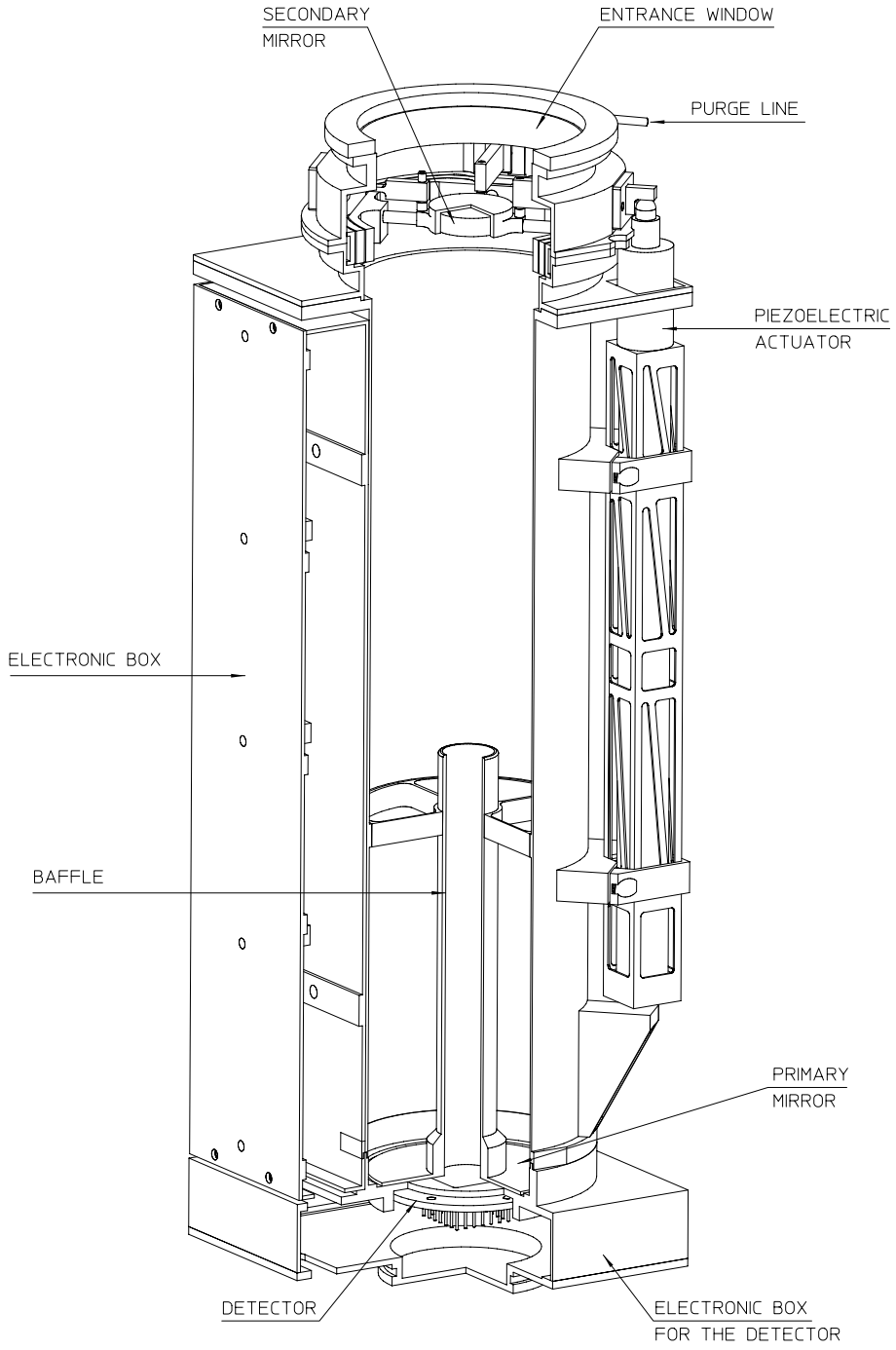

FIGURE 3. Cut-out of the Luminosity Oscillations Imager. The electronic box is located at the outside of the tube. The separation is needed for minimizing the contamination from the outgassing electronics parts and coatings.

Given the sensitivity of the design to the intermirror distance, it is required that the material making the cylinder holding the mirror be insensitive to change in temperature.

Last but not least, the telescope must be able to correct for pointing offset as large as 7 arcmin with a stability better than 0.1 arcsec over 60 sec. The pointing correction can be achieved either with the primary mirror or the secondary mirror. Given the requirement on the compactness of the instrument, it is easier to move the secondary mirror. The choice of the location of the rotation point was also driven by the available room. Although a rotation of the secondary mirror about the focus of the primary mirror would provide a symmetrical aberration (around the chief ray) and a lack of coma, we chose to rotate the secondary mirror around its vertex.

4.4.3. *Telescope: Design*

The telescope is a Ritchey-Chrétien with a 1300-mm focal length. The effective diameter of the telescope is 54 mm, with a central obstruction of 26-mm diameter. The concave primary has a focal length of 289.63 mm and an aspherisation of -1.02 (parabolic). The convex secondary has a focal length of 70.30 mm and an aspherisation of -2.7 (hyperbolic). The focal length f of the mirror is then given by:

$$f = \frac{R}{2} \tag{4.1}$$

The shape of the mirrors is given from the following equation of a conic:

$$r^2 + 2Rz + (1+k)z^2 = 0 \tag{4.2}$$

where r is the radial distance to the mirror vertex, R is the curvature at the vertex, z is the height on the revolution axis (i.e. often the normal to the mirror) and k is the conic constant. It can easily be show from Eq. (4.2) that the surface is a sphere of radius R for k=0 and a paraboloid for k=-1. When $-1 < k < 0$, we have an ellipsoid. When $k < -1$, we have a hyperboloid. Equation (4.2) can be solved to yield z as a function of r:

$$z = \frac{r^2}{R} \frac{1}{1 + \sqrt{1 - \frac{s^2(1+k)}{R^2}}} \tag{4.3}$$

The focal length f of the telescope depends upon the focal length of the mirrors (f_p and f_s) and on the intermirror distance d:

$$\frac{1}{f} = \frac{1}{f_p} + \frac{1}{f_s} - \frac{d}{f_s f_p} \tag{4.4}$$

The focal length is positive for a concave mirror, and negative for a convex. The imposed focal length provide an intermirror distance of 235 mm.

There are several tolerances that will constrain the telescope design. For instance, we wish to impose that the focal length does not vary by more than ± 0.5 due to temperature variations. In addition, the location of the focal plane is to be at 10 mm from the vertex of the primary mirror; this location must not vary by more than ± 1 mm in order to minimize the change in the point spread function (PSF). It can be derived from Eq. (4.4) that the sensitivity of the focal length to the intermirror distance is given as:

$$\frac{\Delta f}{f} = \Delta d \frac{f}{f_s f_p} \tag{4.5}$$

It can also be computed that the distance e of the focal plane from the vertex primary mirror is:

$$e = \frac{(f_p - d) f_s}{f_s + f_p - d} - d \tag{4.6}$$

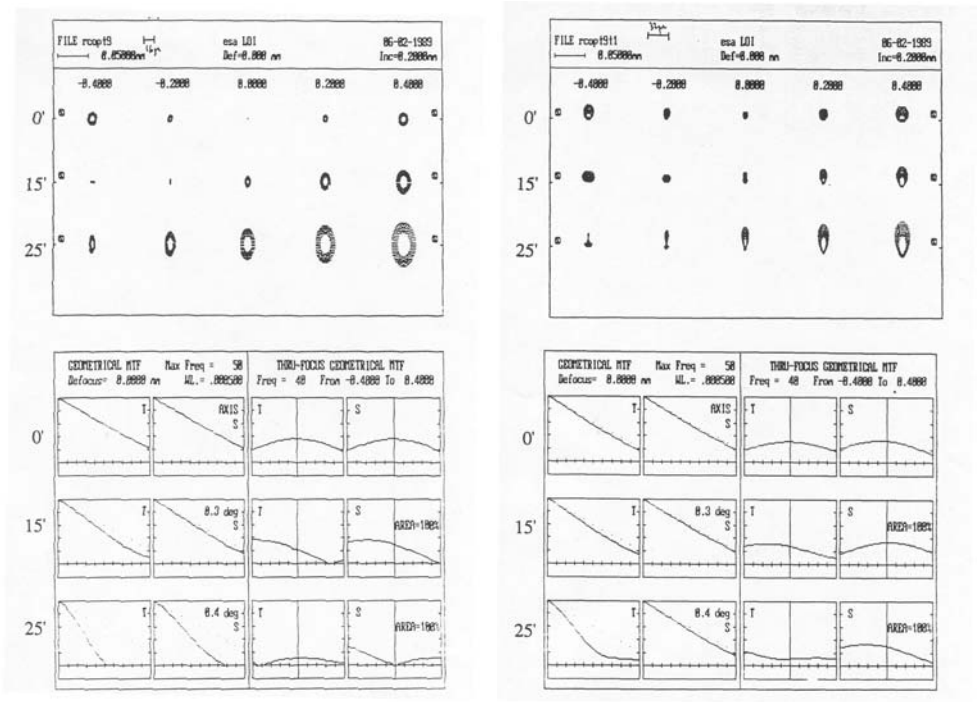

FIGURE 4. Left, spot diagram and Modulation Transfer Function (MTF) of the telescope for an on-axis image, for different location in the field of view, and for various focal plane location. Right, same diagrams for an off-axis image compensated by a tilted secondary mirror. Spot diagram and MTF can be obtained with a ray-tracing programme such as ZEMAX.

From Eq. (4.6), the sensitivity of e to the intermirror distance is given by:

$$\Delta e = \Delta d \left(\frac{-f_s^2}{(f_s + f_p - d)^2} - 1 \right) \tag{4.7}$$

The most stringent requirement from the two is the location of the focal plane that will impose a variation to the intermirror distance not larger than $\pm$ 0.05 mm. Given the temperature variations encountered by the spacecraft of about 20 K, this will impose the maximum CTE that we can tolerate for the structure of the telescope, that is 10^{-5} K^{-1}. The chosen material for the structure is Invar with a Coefficient of Thermal Expansion (CTE) of 0.5 10^{-6} K^{-1}, a factor 18 better than required. Invar is a special type of stainless steel having a higher content of nickel (36%) providing a very low CTE.

This also force to choose mirror material with a low CTE in order to reduce the differential CTE. To minimize this effect, the mirrors are made of ceramic glass Zerodur with a CTE of 10^{-7} K^{-1}. The primary mirror is registered on 3 small Invar pads of 2-mm diameter; they are built in the Invar tube. At the back of the primary mirror, opposite of the pads, three 2-mm diameter pins apply each a 10-N force; this insures that the mirror is kept in place for accelerations up to 30 g. The secondary mirror is mounted with 3 similar pads, but instead of a known force, the ring supporting the pads is just lightly clamped and its holding screws are glued. The secondary mirror is mounted in a gimbal allowing to keep the Sun centred on the detector (See section 4.6.1). The design is such that the Modulation Transfer Function (MTF) of the telescope is not degraded even for a 10' offset of the Sun (See Fig. 4).

Although, we had no requirement for scattered light, we studied the baffles of the

telescope using the APART programme. The main source of scattered light will come from the mirror themselves for which the baffles are of limited use. The design of the internal baffle was such that no direct light from the Sun could reach the detector. The baffle was held in place with a spider in the shadow of the secondary mirror spider. In order to minimize scattered light from the telescope tube, the inside was machined to reduce the surface of the cylinder by removing material in the form of a cutting saw. The tube (and the secondary gimbal) were painted with a low-outgassing paint known as Electrodag 501.

4.4.4. *Filter: requirements*

The design of the entrance filter was to have the following requirements:

- Narrow band (5 nm) at 500 nm
- Entrance window warmer than the structure
- Minimize radiation damage
- Controlled transmission
- Minimize out-of-band light contribution

The spectral selection is performed by a 5-nm passband interference filter at 500 nm, used as an entrance window. The wavelength and passband was chosen as to minimize the amount of solar Fraünhofer lines likely to be sensitive to solar activity. The filter closes the Invar tube and isolate the mirrors and detector from the outside (See Figure 2). The thermal design of the filter must insure that its temperature is hotter than the rest of the structure. This will reduce the risk of condensing contaminants coming from the spacecraft, hence reducing the chance of a drastic drop in transmission due to polymerization. A temperature difference of about 10 K is sufficient to avoid condensation.

Since the filter faces directly the solar particle flux, the radiation damages to the filter should be minimized. The design of the filter should take into account both the thermal and the radiation aspects. The admissible degradation over the nominal mission lifetime should be lower than 90% transmission drop.

The transmission of the filter should be limited in order to avoid reaching the non-linear response of the detector. The transmission will depend upon the choice of material used for the detection, and upon the design of the detector.

Finally, since the solar flux is broadband, the flux outside the narrow passband should be reduced by 10^{-5} compared to the in-band transmission.

4.4.5. *Filter: design*

A transmitting filter with a narrow passband of 5 nm is achieved with multilayer coatings making constructive and destructive interferences. The choice of the wavelength is achieved in a similar way as in Fabry-Perot filter which transmission peaks are given by:

$$k\lambda = 2ne\cos i \tag{4.8}$$

where k is an integer, λ is the peak wavelength, n is the index of refraction of the gap, e is the thickness of the gap, i is the angle of incidence. In the case of a multilayer coating, a low index of refraction material of optical thickness (ne) of half-wavelength thickness is surrounded by sandwiches of quarter-wavelength thick material. The materials used are typically zinc sulfide, cryolite† or the likes. The idea is to deposit in alternance high and low index of refraction, respectively zinc sulfide and cryolite. The peak wavelength λ_0 is then simply given by:

$$\lambda_0 = 2ne \tag{4.9}$$

† Sodium Aluminium Fluoride

The design of interference filters is out of the scope of this course, but one can read with deeper interest MacLeod (1986). The additional transmission peaks obtained at λ_0/k (at shorter wavelengths) need to be suppressed by additional blocking either performed by additional multilayer coatings and/or colored glass.

The overall design of the filter is also constrained by the need to have a warm filter. At the time of the design, there was very little literature on the thermal design of such interference filters. In addition, the filter sandwich was also designed as to minimize the radiation dose reaching the multilayer coatings. The thermal and radiation protection designs are constrained by each other. The thermal solution, studied using ESATAN, is described by Appourchaux and Cislaghi (1992). It requires the knowledge of the thermal characteristics of the glass substrates, the transmission, absorption and reflection properties of the glass and coatings, the thermal boundary conditions and finally the thermal characteristics of the interface. The thermal design of the filter insures that its temperature is hotter that the VIRGO structure by 10 K (Appourchaux and Cislaghi, 1992). The filter is made of 3 different substrates, all are 3-mm thick and from Schott. The first one is a BK7G18 glass, cerium doped and radiation resistant; it is used to reduce the radiation dose and proton flux received by the other substrates and coatings. The second substrate is a GG475 coloured filter which absorbs about 20% of the incoming solar radiation, it is also used to reduce the amount of blue light received by the coating. The coatings making the spectral selection are deposited on the GG475. The last substrate is a BG18 heat absorbing glass, it is used as a back-up in case the coatings reflecting the infrared get degraded. Finally a chrome coating is deposited at the back of the BG18 glass for getting a 7% transmission; this low transmission insures that the detector is used in a linear regime. The design ensures that the out-of-band contribution is less than 10^5.

4.4.6. *Detector: requirements*

The detector was to have the following requirement:

- low resolution sensitive in the visible (@ 500 nm)
- sensitive to low-degree modes ($l < 6$)
- quantum efficiency less than 500 ppm/K
- pixel crosstalk less than 0.5 %
- response uniformity better than 1%
- provide guiding signals
- low noise

The detector is based on silicon that is sensitive in the visible. The number of pixels was limited to 12 in order to reduce the burden of the read-out electronics. The sensitivity to low degree modes is related to the geometry of the 12 pixels. The temperature dependence of the quantum efficiency of the silicon detector should be minimized for reducing the impact of the temperature variations on the intensity measurements. For instance, a peak-to-peak variation of 1 K would provide a 80 ppm rms variation of the measured intensity or when translated in terms of a white noise background in a power spectrum 0.4 $\mathrm{ppm}^2/\mu\mathrm{Hz}$. The crosstalk between adjacent pixel should be kept to a minimum. The detector will also provide the guiding signals thereby ensuring that the solar image will properly centered onto the detector, and that guiding noise will be minimized. Finally, the detector was used as a current generator (photovoltaic mode) and was not polarized by a bias voltage. This is for a getting a lower noise and for avoiding to control to a few ppm the bias voltage.

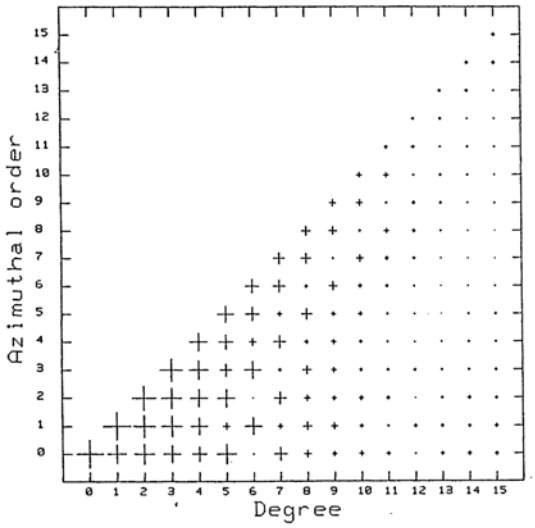

FIGURE 5. Response of the detector to spherical harmonics function as a function of the degree and of the azimuthal order. This configuration offered the best compromise between sensitivity to $m = l$ modes and $m = 0$ modes.

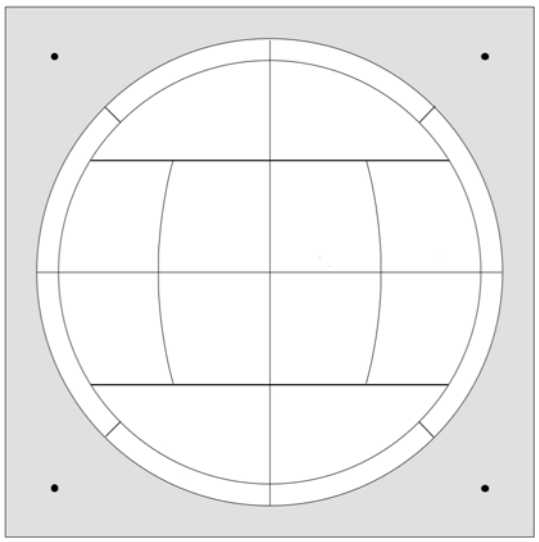

FIGURE 6. LOI detector optimized for the detection of low degree modes. The guiding pixels are 4 quadrants of an annulus with an inner and outer radius of about 0.95 and 1.05 solar radius, respectively. Each guiding pixel is physically and electrically divided in two pixels for redundancy purposes. The four black spots at the corners are the temperature diodes. These diodes are below an aluminium layer shown here in grey.

4.4.7. *Detector: design*

The configuration of the 12 scientific pixels shown on Fig. 6 was optimized by Appourchaux and Andersen (1990). The sensitivity of that configuration to the modes is

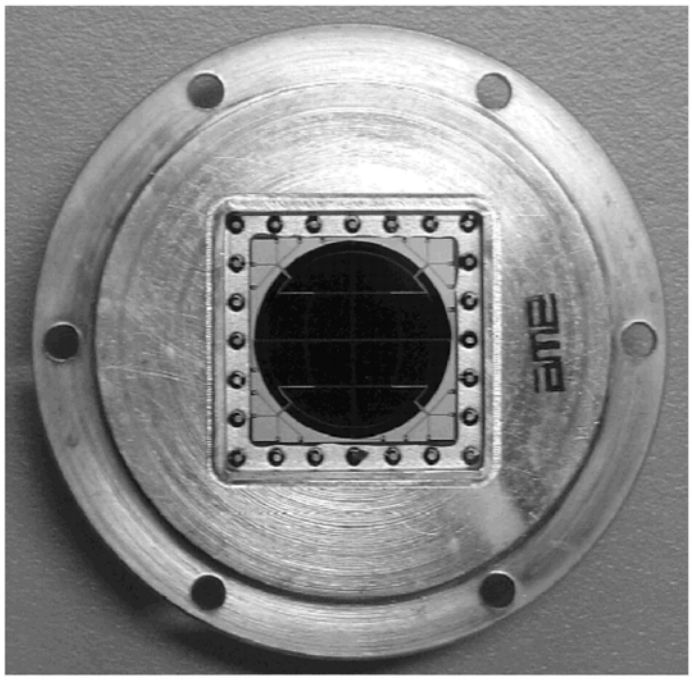

FIGURE 7. Photo of the LOI detector in its flight case. The Kovar case is soldered to a Kovar mounting plate that is bolted at the back of the telescope tube and isolated from the tube with an Ertapeek washer. The 100-μm wide tracks are easily seen.

shown on Fig. 5. Other effects related to sensitivities to guiding offset can also be found in Appourchaux and Andersen (1990).

In order to optimize the temperature dependence of the pixels, several different processes were tested (See Section 4.9.4). After selection of the best process, the photodiodes were deep diffused p-n junction with an epitaxial substrate (low resistivity). In addition 4 temperature diodes are built in the detector for having the temperature across the substrate (See Fig. 6). These temperature diodes provides a signal in photovoltaic mode that is proportional to temperature. For improving the definition of the sensitive area of the scientific pixels, a layer of aluminium is deposited outside the pixels and over the temperature diodes. In addition, each pixel and each temperature diode is surrounded by a n^+ deep diffused guard ring; this will minimize the crosstalk between the pixels. It will also insure that the signal of the pixels do no get contaminated by a pixel for which the bonding wire breaks; in this case the electrons flow to the ground and not the other pixels. Each guiding pixel is made of two independent pixels that are connected to the same output (Figure 7). In case one of these pixels would not be functional, we would still have guiding information and the image of the Sun would have a slight offset.

4.4.8. *Guiding system: requirements*

The guiding system is the critical part of the LOI. The design of guiding system was to have the following requirements:

- Pointing noise 3 times lower than solar noise
- Gross and fine pointing
- Survive launch vibrations

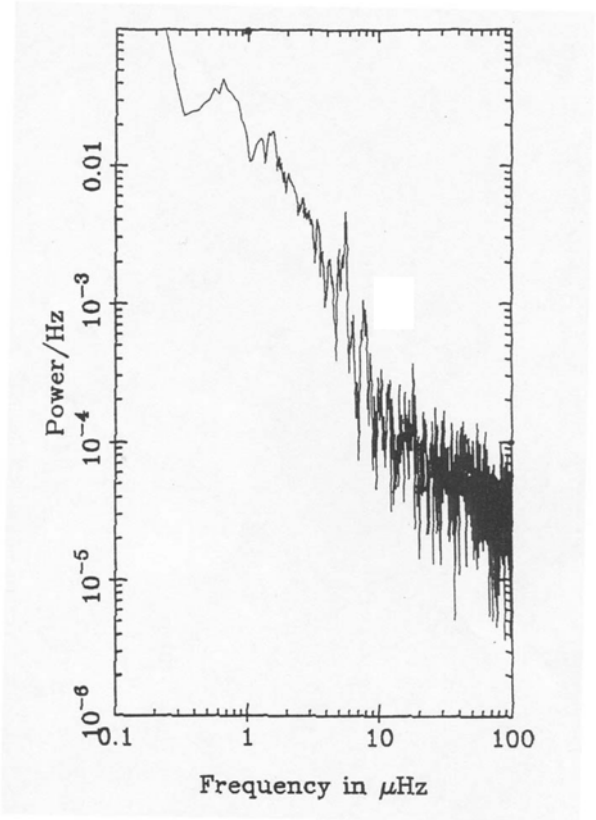

FIGURE 8. Power spectrum of the IPHIR instrument in the g-mode range. The power spectrum is only limited by the solar noise.

- Long lifetime

The first requirement is related to the fact that since we make an image of the Sun on a low-resolution detector, the pointing jitter will introduce noise due to the solar limb darkening that can amount up to 1000 ppm/arcsec (Appourchaux and Andersen, 1990). At the times, measurements made by IPHIR aboard the Phobos spacecraft was the only reference of the level of the measured solar noise (Fröhlich et al., 1988b). The typical solar noise was about 0.36 ppm^2/μHz @ 3 mHz (p-mode range), and 100 ppm^2/μHz @ 100 μHz (g-mode range) with ν^{-2} dependence to the power spectrum in that range. This would set the level of the power spectrum to 0.04 μarcsec^2/μHz @ 3 mHz (p-mode range), and 11 μarcsec^2/μHz @ 100 μHz (g-mode range). After integration over the whole spectral range, the rms pointing jitter should be lower than 0.12", that can be roughly translated by a peak-to-peak value of 0.7" (6 times larger). This requirement is to be achieved at the level of the detector, that is after compensation by an eventual close loop system, and after integration by the electronics.

According to the SOHO EID-A, the variation of the absolute pointing between on-ground alignment and end of nominal mission is better than 5 arcmin (3 σ value), while the relative pointing accuracy is better than an arcsec over 15 minutes, and better than 10 arcsec over 6-months. The latter is out of the requirements set by the solar noise. An active pointing system is therefore required to reduce the 10-arcsec figure to less than an

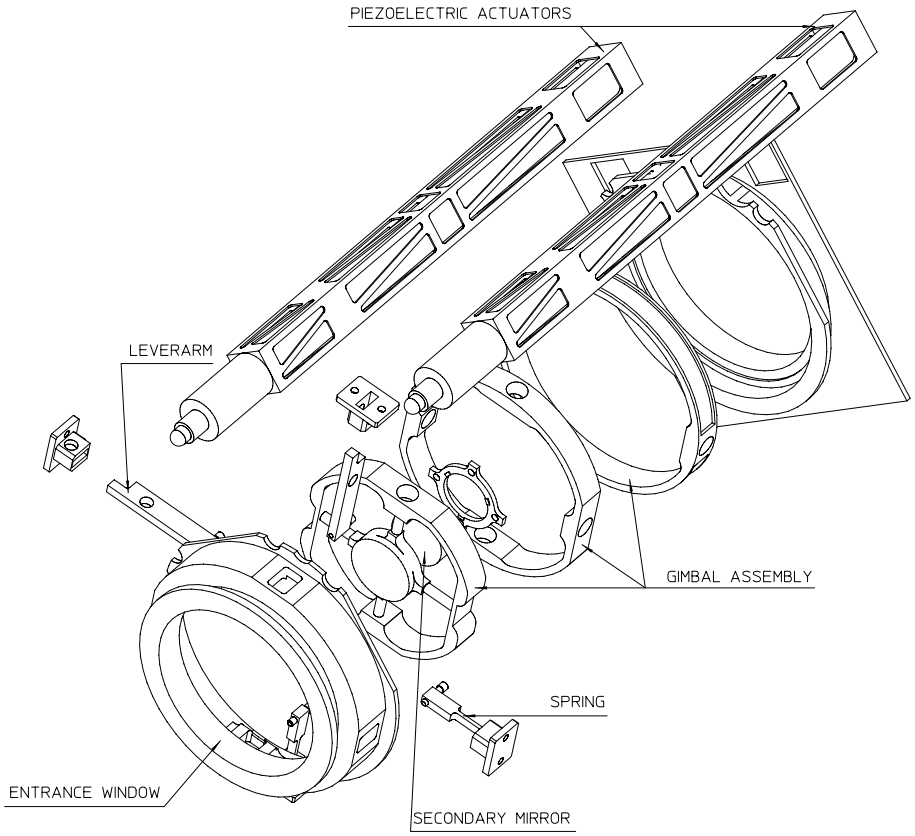

FIGURE 9. Artistic blow-up of the guiding system. The assembly of the 3 rings making the gimbal is very critical. Friction between the rings modify the normal behaviour of the guider. The piezoelectric actuators are longitudinally kept in place by back screws, not shown here. For each axis, the fine adjustment is made with a screw located on the lever arm. The 20-N force is adjusted with a screw located on the spring arm.

arcsec. The guiding system must be able to cope with large misalignement (arcmin) as well as finer and faster jitter (arcsec).

As soon as the requirement for a mechanism is set, there is the obvious need that this mechanism be able to survive the vibrations encountered by the launch. And of course, the mechanism being needed for achieving the scientific objectives there is the additional requirement that the guiding system be able to function during the de nominal mission and beyond.

4.4.9. *Guiding system: design*

The guiding system is based on the following principle: 2 piezoelectric actuators rotate 2 lever arms that push on a gimbal in which the secondary mirror is mounted. The rotation of this mirror is done around its vertex. Two spring arms opposite of the two lever arms provide a restoring force (about 20 N) and act as a locking mechanism (Figure

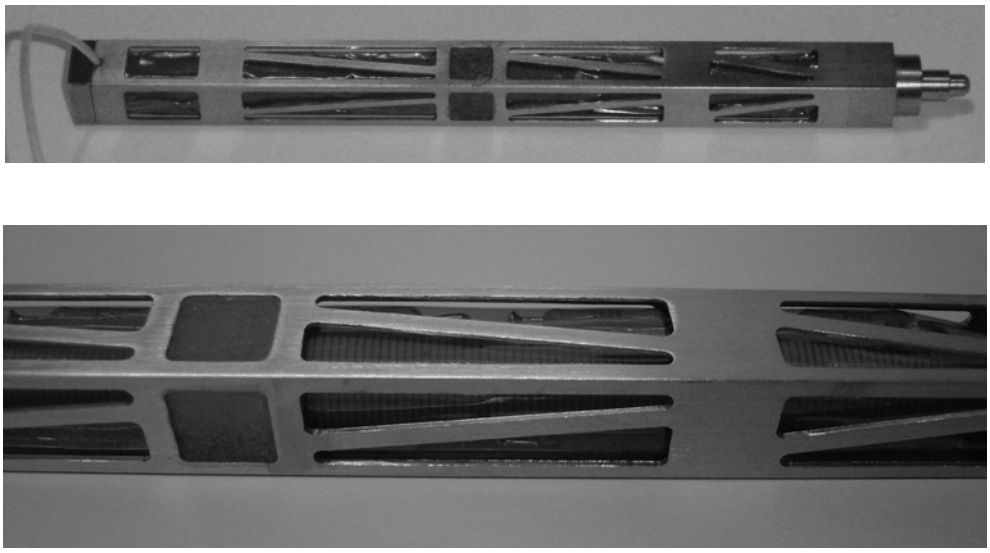

FIGURE 10. Photos of the piezoelectric actuators. Top, the actuator is about 230 mm long. For saving mass the case is ribbed. The actuator is held laterally at the back by a screw pushing into an hemispherical cut-out, in the middle by a bracket and at the top by a square cut-out in the mounting frame. The ball end of the actuator pushes onto a flat part of the lever arm. Bottom, enlarged view of the central part of the actuator. This is where can be seen each disc making the actuator, and also where the stack is held by a potting material. This will considerably reduce the amplitude of the lateral motion of that part during vibrations.

9). In order to compensate for 1 arcmin off pointing on the detector, the secondary mirror needs to be rotated by 2.65 arcmin. This is due to the larger apparent size of the solar image as reimaged by the secondary mirror.

For coarse guiding, the total range needed is ±7 arcmin. This is for allowing for the long term drift of the spacecraft (±5 arcmin), the temperature setting of the actuators (±1 arcmin†) and alignment errors of the entrance filter (±1 arcmin). The required extension d of the actuator is given by:

$$d = re\frac{A_s}{a_l}\frac{1}{C(K_s, K_l, K_p)} \tag{4.10}$$

where r is the required range (± 7 arcmin), e is the distance of the lever arm, pushing on the secondary mirror mount, to the vertex of that mirror (=12 mm), A_s is the amplification giving the actual range at the secondary mirror (=2.65), a_l is the amplification of the lever arm (the piezoelectric actuator pushes on the other end of the lever arm with a reduction factor of 2.25), C is a reduction factor taking into account the stinesses of the actuator K_p, of the lever arm K_l and of the spring arm K_s. Unfortunately, the varying load seen by the actuator will reduce the effectiveness of the extension. The reduction factor is given by:

$$C(K_s, K_l, K_p) = \frac{K_l}{K_l + K_s}\frac{K_p}{K_p + \tilde{K}} \tag{4.11}$$

where $\tilde{K}$ is the equivalent stiffness of the spring arm at the level of the piezoelectric

† corresponding to 0.5 μm/K

actuator given by:

$$\tilde{K} = a_l^2 \frac{K_s K_l}{K_l + K_s} \tag{4.12}$$

The guiding system had also to be designed bearing in mind that it must survive launch vibrations. The rôle of the spring arm is to provide a restoring force as well as to serve as a locking mechanism. The reduction of extension as given by Eq.4.11 was imposed to be less than 15%. This sets the requirements on the stiffness of the spring arm and lever arm system. Therefore according to Eq. 4.10, the extension of the actuator should be at least 68 μm.

There are two additional design constraints that needs to be taken into account: the operating voltage and the failure scenario. These two constraints are related to the design of the piezoelectric actuator themselves. The actuator are made of about 240 elements of lead zirconium titanate (PZT) that are about 1 mm thick each. They are soldered back to back with 240 electrodes providing the electrical polarization for each element. The length of the 240-disc stack is about 230 mm. To avoid to break the stack during launch vibrations, the middle of the stack is strapped to the case over 10 mm; this design is qualified for the launch of SOHO (See Figure 10). The failure mode of a single element will give a short circuit. Since all the elements are fed in parallel this would destroy the output of the voltage power supply. In order to avoid such a failure modes, it was decided to construct the actuator as a sum of 12 independent actuators by putting a resistor in serie of the 20 elements. The failure of one element would reduce the extension by 1/12. Therefore the extension of the actuator should be at least 74 μm. Last, the maximum operating voltage of the actuator is typically 700 volts. At the time of design, lower voltage, say 100 volts, would have implied thinner piezoelectric elements in the same ratio. These were considered still in the development stage for space application and the choice of having low-voltage was therefore not an option. We chose to operate for derating reason at a maximum voltage of 600 volts. This then induced a further extension reduction compared to the 700 volts operation. The final requirement for the actuator extension was then 86 μm at 700 volts.

The force applied by the spring arm is used as a locking mechanism. This is a passive lock and there is nothing to unlock. The complete guiding systems comprising the spring and lever arms, the two piezoelectric actuators, the gimbal rings (inner and outer) was subject to a finite elements model (f.e.m) analysis performed with NASTRAN. This analysis permits to describe the mechanical behaviour of the system under various static and dynamical loads. The goal of that analysis was to assess whether the guiding system would survive launch (e.g. avoid gapping at the actuator level that could cause destructive shocks), and estimate the resonance frequencies of the guiding system that could lead to instabilities for the closed loop system. The f.e.m. analysis confirmed that the spring arm would effectively act as a lock, and that the first two resonances frequencies (250 Hz, 380 Hz) would be high enough for not being excited by the servo loop system

For the fine guiding, the error signals, provided by the guiding pixels, are fed back to the high voltage power supply that drives the actuators. The guiding regulator is an integrator. The cut-off frequency of the complete guiding system is 10Hz @ 3dB.

Finally, the long lifetime was ensured by using Bendix free-flex pivots that provide rotation using a flexure mechanism. In case of a space application, ball bearings are to be avoided at all cost to the long continuous operation and likely wear occurring in such mechanism. In addition, ball bearing are considered dirty because of the use of a lubricating medium likely to outgas hydrocarbons. The free-flex pivots are shown on Fig. 11.

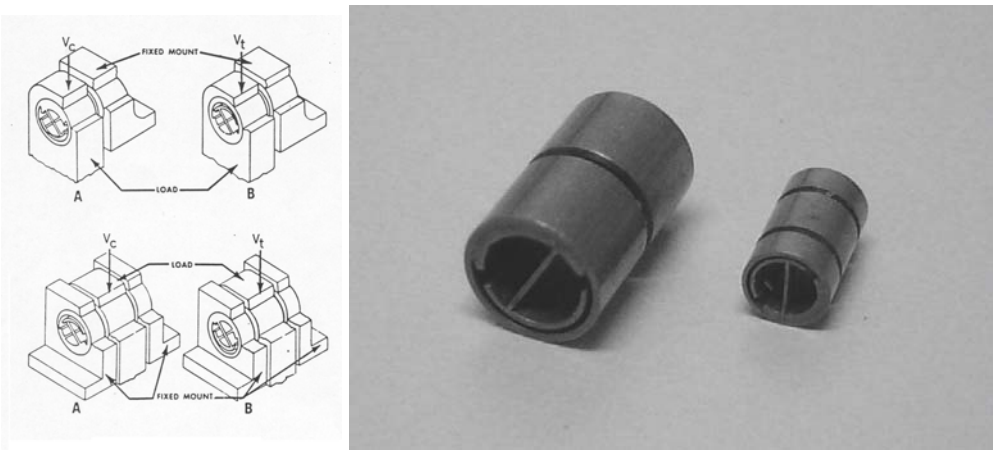

FIGURE 11. The Lucas (formerly Bendix) free-flex pivot provides rotation up to $\pm$ 30 degree, without friction. The pivot is made of flat, crossed springs supporting rotating sleeves. There are two kinds of pivot: cantilevered (used in the gimbal, cartoon at left, top; and photo at left); double-ended (used for the lever arms, cartoon at left, bottom; and photo at right)

4.4.10. *Electronics: requirements*

The electronics was to have the following requirements:

- low noise
- long integration time
- high voltage power supply
- guiding servo loop
- provide housekeeping signals

The first requirement is obviously related to the tiny variation intensity measured on the Sun (ppm).

The second requirement is related to the sampling criterion of Shannon. When one wants to reconstruct an analog signal with a digital one, it is required that the sampling time be twice shorter than the highest frequency to be recovered, i.e. if one wants to access the highest frequency corresponding to a 2-minute periodic signal, one must sample the signal to 1 minute. Unfortunately, it is never mentioned anywhere how the sampling should be performed. As a matter of fact, a shorter integration time compared to the sampling time will considerably 'fold' in high frequency noise. It is then essential that the integration time during the sampling interval be optimized to be as long as feasible, i.e. the integration cycle should be close to 100%.)

The electronics should also provide the guiding analog loop by taking the error signals from the detector and fed them back to the actuators via a high voltage power supply driving them. The overall design of a control loop is well known but still great care should be taken for avoiding to have an unstable closed loop system.

Last several housekeeping signals such as temperatures, high voltages are needed to make sure that the instrument performs as expected.

4.4.11. *Electronics: design*

For low noise, the 12 scientific pixel currents are converted into voltages by 12 low-noise operational amplifiers (AD-OP97) in a zero bias configuration. This latter will minimize the $1/\nu$ noise. The analog-to-digital conversion is performed by synchronous VFCs (AD652). VFC are intrinsically more stable than Analog-to-Digital converter because the reference is no a voltage but the frequency of a quartz. The VFCs are

co-located on an aluminium-oxide substrate (hybrid technology) for improved thermal stability. The VFC outputs are accumulated into 24-bit counter ASICs (Application Specific Integrated Circuit). The integration time is 99% of the sampling time of 60s. The ASICs are read by the VIRGO Data Acquisition System (DAS) (Fröhlich et al., 1995). The resolution of the data chain is better than 0.1ppm.

The guiding pixels are amplified in the same way as the scientific pixels. The North-South and East-West guiding errors are obtained using differential amplifiers. The error signals are fed into servo regulators driving high voltage output stages (bipolar discrete technology). The high voltage amplifiers have a fixed gain. They are built with high voltage DC/DC converters with a fixed output voltage (600 Volt) and series regulator circuits. The negative lead of the actuators is kept at a constant voltage of 150 Volt. The positive lead is variable between 0 and 600 Volt. If needed the servo loop can be switched off and a fixed voltage can be applied to the actuators. The fixed voltages are selectable by telecommands. The servo loop regulator is of the proportional-integral type (PI, order 2 servo loop). This type of servo loop provides a zero steady-state pointing error. The closed loop characteristics of the servo is a first order low pass with a corner frequency of 10 Hz with a phase margin of abut 65 degrees.

4.5. *Integration*

At this stage of the game, each subsystem is defined with its own set of requirements. The subsystems have to be assembled together. This assembly requires the definition of interfaces for each subsystem. These interfaces can be mechanical, thermal or electrical. The interface definition can be somewhat complex and subject to extensive discussions or even negotiations. In the case of the LOI, the internal interfaces were defined by the LOI team, while the external interfaces (with the PI instrument) were defined with the VIRGO team (See Fig. 17). Then at a higher level, the VIRGO team defined the interfaces to the SOHO spacecraft in agreement with the SOHO project (See Fig. 18).

The main objective when defining the internal LOI interfaces was to ensure that the requirements imposed on each subsystem would not be degraded by the whole assembly. For instance the primary mirror was mounted on 3 small pads machined inside the invar body. The primary mirror was held in place on the 3 pads by three opposite spring-loaded pads pushing at the back of the mirror with a predetermined force. Mounting tolerances ensured that the primary mirror would not move by more than 100 μm axially on the pads. The secondary mirror had similar pads but instead of force applied by spring, a ring holding the pads was lightly clamp and its screws glued. This simple minded approach was simple and effective as shown by the telescope test. A similar approach was used for mounting the entrance filter. The case of the actuators is clamped for avoiding lateral motion, while a screw at the back of the actuator serves as for reference and for adjustment. The detector is directly mounted into a Kovar plate which is bolted on the Invar structure behind the primary mirror. The ground lead of the detector is connected to the Kovar plate, and this plate is isolated from the Invar using an Ertapeek washer.

The contamination program put in place for avoiding to contaminate the optical instruments, especially the instruments working in the UV and EUV, placed additional design constraints on the geometry of the instrument. For instance, it was suggested in the Experiment Interface Document Part C (SOHO EID-C) that the optical part of the instruments be physically separated as much as feasible from the electronics. The rationale for that suggestion was related to the large quantity of potential hydrocarbons contaminants present in the various electronic coating and parts. This suggestion was implemented in the LOI by having the invar tube nearly hermetical to the outside closed

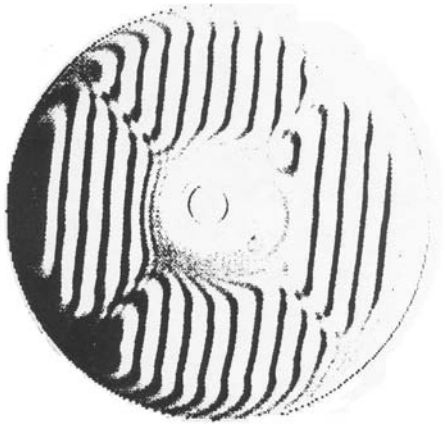

FIGURE 12. Interferometric tests of the telescope performed in a clean room having a Zygo interferometer. The interferometric test consist in making the interference between a reference beam and the beam as transmitted by the telescope in our case going through the instrument twice. The interferences resulting are fringes that are supposed to be perfectly straight if the telescope is perfect; any deviation to the straight line provides information about the optical quality of telescope. That optical quality is usually referred to the wavelength of test (here a helium-laser at 632.8 nm) that sizes the wavefront deformation. In the case of the LOI, that wave front deformation is not worse than $\lambda/30$ rms in double passage. The four spokes of spider holding the secondary mirror are clearly.

by the entrance filter and by the detector; the only openings were the necessary gaps for the two lever arms (See Fig. 3 and 2). The two other suggestions of the SOHO EID-C was to have an entrance window warmer than the structure (already implemented) and a cover. The warmer window reduces the amount of material that could be condensing on the entrance window. The cover is used for sunlight protection during critical operations (thruster operations generate plumes of hydrazine surrounding the spacecraft), but also is used for letting the whole instrument getting cooked and outgassed during its journey to the L1 Lagrangian point. The overall cleanliness requirement of the SOHO programme imposed severe constraints on the daily integration activities in the clean room. A constant monitoring of the dust particle and of the hydrocarbon contamination must be maintained. In addition, all parts are to be packed in a clean material that was simply regular aluminium cleaned and wiped with chloroform. Last but not least, all electronic parts and paints are baked at high temperature and in vacuum for reducing the amount of outgassing material they may contain.

Finally, another simple requirement is that the integration of the instrument be as simple as possible. This requires the interaction of many actors in the team to arrive at a sensible integration design.

4.6. *Testing*

The testing of the instrument is related to the derivation of its intrinsic performances and to its calibration. It ensures that the scientific and technical requirements are achieved. But the testing is also related to the simulation of the environment of the mission (vibrations, thermal, radiations, etc...). Either type of test can be achieved at instrument level or at sub-assembly level.

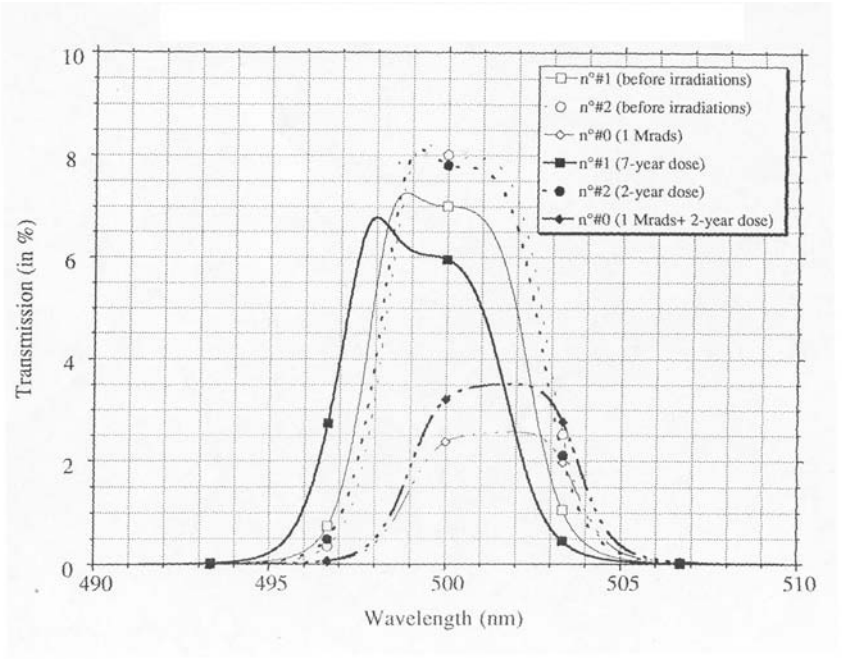

FIGURE 13. Two filters were irradiated with protons simulating a 2-year and 7-year dose. The degradation is not negligible for the 7-year dose providing a 15% transmission drop and significant passband shift. These two effects shows that both the glasses and the coatings were damaged by the irradiations. A third filter was irradiated with γ rays and with a 2-year proton dose. The apparent increase in transmission is due to the annealing (or recovery effect) of the irradiations since a the proton irradiation took place a few weeks after the γ-ray irradiation.

4.6.1. *Telescope*

The telescope was subject at instrument level to interferometric tests. The tests were performed with the mirrors integrated in the overall structure and with the mounting scheme mentioned above. The tests were performed on axis, i.e. the secondary was not tilted. Figure 12 shows the results of the test. The optical quality is better than $\lambda/30$ rms.

The focal length of the telescope was measured using a collimator with a focal length known to better than 0.005%. It allowed to measure the focal length of the telescope to better than 0.06%.

4.6.2. *Filter*

The main concern for the entrance filter was its ability to survive under solar particles irradiations. γ-ray irradiations of the various glass were performed. It resulted in the understanding of how the irradiations would increase the absorption of the glasses by creating color centers (Appourchaux et al., 1994). The tests performed under γ-ray irradiations are rather easy to implement. But in order to be more realistic, it was also necessary to irradiate the filter with protons. The main difference is that in the former case the dose is deposited homogeneously throughout the thickness of the glass, while for the latter the dose deposited will depend upon the energy of the proton. For protons, the dose will increase as the proton loses energy inside the glass thickness. Tests performed under protons irradiations simulating the 6-year SOHO radiation dose showed that the filter would survive the mission as shown in Fig. 13 (See also Appourchaux, 1993).

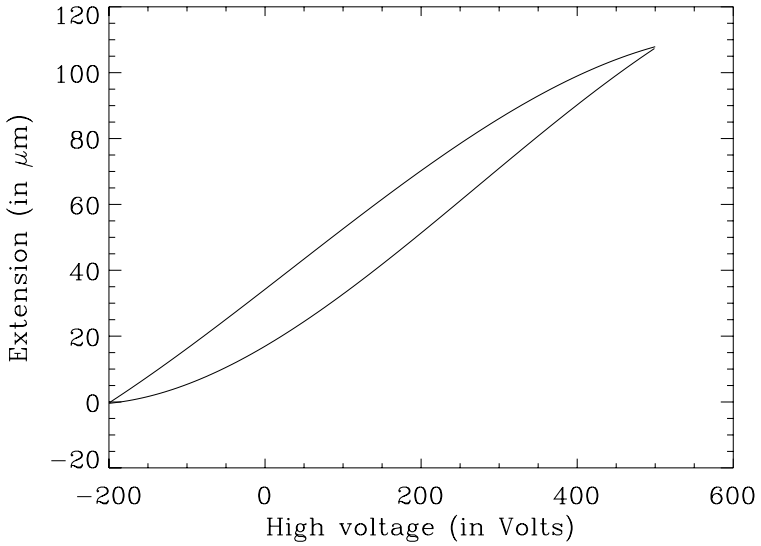

FIGURE 14. Extension of the piezoelectric actuator as a function of voltage. The hysteresis is an effect due to the property of PZT: the extension is different when the voltage is increased and then decreased, or vice versa. The hysteresis effect can be compensated by measuring the absolute extension of the actuator with capacitor sensors.

In addition, the filter after a 1-year dose of UV irradiation showed no significant sign of degradation either in its absorptance (Marco et al., 1994) or spectral characteristics.

4.6.3. *Guider*

We encountered a major difficulty when making the guider functions properly. We found out that the assembly procedure for mounting the 3 rings making the gimbal system needed to set such that there was no friction between the rings. The slightest amount of friction would prevent the gimbal to rotate properly making the system extremely non-linear. In addition, the pivots are mounted in the rings with shear force making the gimbal almost impossible to disassemble if a problem is encountered. After setting the proper mounting procedure (using shemes) the guider can be fully assembled in the invar tube with the actuators and the lever and spring arms. The overall alignment procedure is rather delicate as a predetermined force has to be applied by the spring arm to act as a locking mechanism: too little force may break the actuator during launch, too much force would prevent the actuator from rotating the gimbal ring.

Each actuator was also tested for its extension. Figure 14 shows a typical response of the actuator extension. The response will differ depending whether the high voltage was increase or decreased, this is the hysteresis effect of the piezoelectric material. This effect has no impact on the servo loop of the guiding. The only impact is in the reproducibility of the voltage needed for aligning the telescope.

The servo loop of the guiding system was tested with an external optical stimuli that was *static* with respect to the telescope. The effectiveness of the servo loop was tested by injecting *directly* a fake electrical error signal. The test performed this way validate the electrical functioning of the servo loop, and allows to derive the characteristics of the filter required for providing the correction signal (integrator or multiple pole filter). The dynamic characteristics of the guiding system is then fully determined, and there is

no need to provide a *dynamic* optical stimuli because to the response of the servo loop system is the same to the first order. Such a *dynamic* stimuli would only be needed if the response of the optical system would strongly be non-linear. In the case of the LOI, the non-linearities of the optical system are manifest for time scales of the order of months not seconds.

4.6.4. *Detector*

The choice of the detector substrate was the subject of an extensive study implying the testing of several type of junction. A photodiode is nothing less but a junction that is exposed to the light. Given, the bandgap of silicon that is about a few eV, photons falling on the junction will free a hole-electron pair that may travel the junction depending of the energy of the photons and on the strength of the electrical field across the junction, the latter depending on whether the junction is polarized or not. The modelling of the quantum efficiency of a junction is not a very complex affair whereas the prediction of its dependence upon temperature is much more difficult. That is the main reason why several type of junction were fabricated and tested as can be attested by Appourchaux et al. (1992). The different processes tested were the following:

- Deep diffused p-n junction on 10 Ω.cm material
- Ion implanted p-n junction on 10 Ω.cm material

each grown on material with the following characteristics

- 10 Ω.cm material
- 100 Ω.cm material
- epitaxial material (low resistivity)

The processes on epitaxial material had also n^+ deep-diffused guarded ring around the temperature diodes and the pixels; and also an aluminium layer deposited outside the pixels above the sensitive area. In total more than 35 detectors were tested. The spectral dependence of the temperature coefficient of the quantum efficiency was reported by Appourchaux et al. (1992). We also measured the crosstalk between neighboring pixels, i.e. the amount of hole-electron pair flowing from one pixel to the other. Figure 15 show a typical example of a crosstalk response that measured to be less than 0.03% when using guarded ring. The process chosen for the flight models was the *Deep diffused p-n junction on epitaxial material*. The main advantage is that this process is inherently more stable than that of the ion implanted. Additional tests included the calibration of the photoresponse of the photodiode (in A/W) using a calibrated radiometer. The tests on the Flight Models showed that the temperature dependence of the detector was less than 50 ppm/K @ 500 nm.

4.6.5. *Electronics*

The stability of the VFC was measured using a stable voltage supply. The results showed that the output noise on the digital signal was 6.3 10^{-5} ppm^2/μHz @ 3 mHz, and 10^{-2} ppm^2/μHz @ 100 μHz. This stability is about at least a factor 100 less than the solar noise. This noise sources were the stability of the voltage standard used for calibration, and the temperature coefficient of the VFC which was about 1.5 ppm/K.

As mentioned above the guiding servo loop electronics was set during a system test of the whole guider. Additional tests included the measurement of the impedance of the actuators. The impedance of the actuator introduces phase gain that needs to be taken into account in the design of the servo loop.

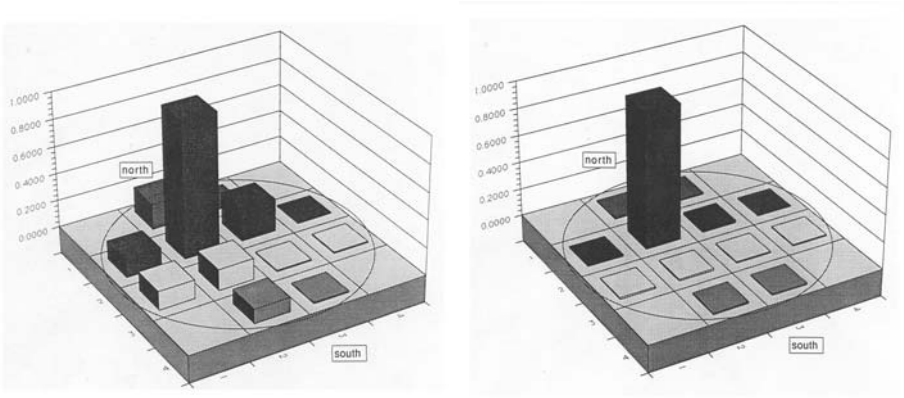

FIGURE 15. Crosstalk measured on the detector: left, for deep diffused p-n junction on 100 Ω.cm; right, for deep diffused p-n junction on 10 Ω.cm. The maximum crosstalk is 18% and 1.3% respectively. These detectors had no guarded ring around the pixels explaining the larger crosstalk measured, and hence justifying the need for such a guarded ring.

4.6.6. *Instrument level test*

The tests performed at the level of the instrument are of several nature. The launch is simulated by vibrating the instrument on a hydropneumatic pot that can simulate either the sinusoidal loads or random loads. The electromagnetic emission (EMI) and susceptibility (EMC) are tested to ensure that the instrument does not radiate too much for the other instruments of the payload, and the other instruments will not induce noise inside the instrument. Finally, the thermal conditions encountered in space are simulated in a thermal chamber and in vacuum. All these stringent tests should not affect the performance of the instrument.

These tests are performed at two level: qualification and acceptance. The qualification levels are usually higher and more stringent (larger load, larger temperature range) than the acceptance levels. The Qualification Model of a space instrument is almost like a Flight Model. The former was subjected to qualification levels while the latter was subjected to acceptance levels.

The LOI programme followed the path: Structural Model, Electrical Model, Qualification model, Flight model and Flight Spare. This is referred as the Model philosophy. For some faster programme, only an Electrical Model and a Flight model (called Proto-Flight) are built. The choice of the model philosophy is a choice only based on trade-off between risk and speed. In the case of the LOI, there was no risk taken. The tests performed on the Qualification Model (QM) were very stringent. For instance, the QM had to be vibrated twice to qualification levels because the first time the screws of the guiding system were not properly locked by glue. Finally, the QM was used for checking the scientific and technical performances of the LOI. It was installed in Tenerife on May 2nd, 1994. The QM permitted to show that the instrument was well designed and gave an insurance that the space instrument would perform equally well. The LOI QM was the first instrument to detect the p modes in intensity from the ground; all modes above $l = 0$ were detected (Appourchaux et al., 1995c). The results provided by the LOI QM are reported in Appourchaux et al. (1995c), Appourchaux et al. (1995b), Rabello-Soares et al. (1997a) and Rabello-Soares et al. (1997b). The QM was nominally operated without any malfunctions until the summer 2000 when it was decided that it would not give

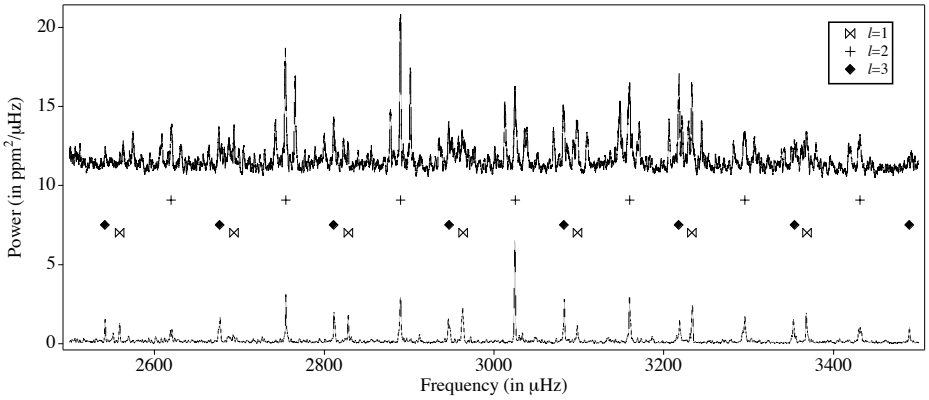

FIGURE 16. Power spectra in the p-mode range obtained for $l = 1, m = 0$ with the QM instrument (shifted by +10 ppm$^2/\mu$Hz) compared to the FM instrument (unshifted). The atmospheric noise is the main source of noise for the QM. It demonstrates what we need to go to space. The daily interruption (day-night) can be seen as frequency aliases of the main peaks in the power spectra for the QM; two aliases are visually detectable. The uninterrupted view of the Sun does not introduce such aliases in the power spectra for the FM. Please note that the $l = 0$ modes are filtered out by the spatial mask.

any additional science return compared to its space counterpart. The spectrum obtained with the QM is compared to that of the FM on Fig. 16.

4.6.7. *Calibrations*

In addition to all the tests performed above, calibration are also required. Calibrations needed are the following:

- Preamplifier-VFC chain (counts to Volts)
- Pixel-preamplifier (Volts to A)
- Quantum efficiency (A to W)
- Temperature sensors (counts to degree)
- Actuators (counts to Volts)
- Guiding (Volts to arcmin)

These calibration are used for converting counts (so-called level-0 data) to engineering data (so-called level-1 data). The next step (level-2 data) involved *a* posteriori corrections related to the actual functioning of the instruments or to specific scientific massage.

4.7. *Operations*

After integrating the LOI in the VIRGO structure (Fig. 17), the VIRGO instrument is then integrated in the SOHO spacecraft (Fig. 18). The SOHO spacecraft is then put atop the rocket (Atlas-Centaur). The launch occurred on December 2, 1995. Simpler written than done. These sequence of events are usually extremely time consuming due to the great care necessary in these last steps. The launch is of course the riskiest part of the whole mission but when that hurdle is passed the mission and operation can start.

The operation of the LOI is rather simple: switch on and observe. There is an other mode that allows to disengage the servo loop system, and to apply a fixed voltage on the actuators. The story of the LOI cover that could be opened on the Christmas eve

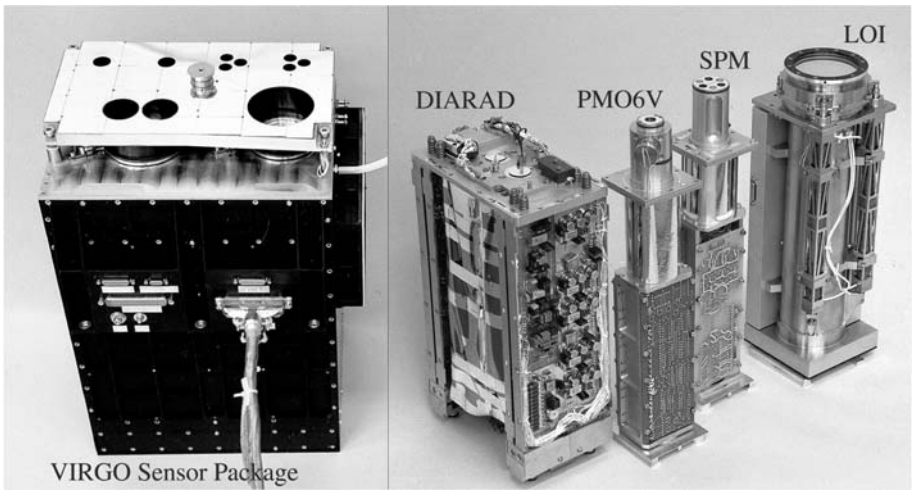

FIGURE 17. The VIRGO instrument shown at left is made of several sub-units: 2 radiometers (PMO6, DIARAD), 3 color sunphotometers (SPM) and of the LOI.

FIGURE 18. Photo of the Sun-facing part of the SOHO spacecraft where VIRGO is integrated. The largest opening is the LOI instrument.

of 1995 but then that could not be opened 2 weeks later is well known by the SOHO community. The complete description of how and why the LOI cover was opened almost

3 months later (on March 27, 1996) is described in Appourchaux et al. (1997). Here, I would not like to expand on the marvellous power of the intellect over matter but this is clearly a simple example of how to solve remotely a problem without sending an astronaut. Of course, this *success* story is much less known (and rightly so) than the recovery of the spacecraft by the SOHO operation team in the summer 1998 (See ESA press release 33-98†). It shows that a well designed spacecraft (and instrument) can survive the most severe environment. From the whole payload complement, only one sub-unit of an instrument could not be operated after the so-called SOHO vacations of 1998. Here I must point out that the LOI survived the severe cold and high temperature to which it was exposed during these SOHO vacations.

Finally, the LOI has been performing without a glitch for the past 8 years. It is likely that this will still be the case at the time this article goes to press. At the time of writing, it is anticipated that the SOHO spacecraft shall be operated until 2007, that is a full solar cycle compared with the initial 2-year mission.

4.8. *Performances and science*

The performance of the LOI were reported by Appourchaux et al. (1997). Since then very little has changed (See Fig. 19). For instance, the SOHO pointing has been remarkably stable providing short term variations of the order of 0.1 arcsec p-p. This stability allowed to detect the solar p modes in the high voltages feeding the actuators but also in the guiding pixels themselves (See Fig 20 Appourchaux and Toutain, 1998). The signal measured in the high voltage corresponds to an error signal of a few milliarcsec (corresponding to a few mVolts or a few Å of extension) at a p-mode frequency.

The temperature stability provided by the spacecraft has also been quite remarkable. The yearly temperature effect due to the varying SOHO-Sun distance is about 3 K p-p. Over periods of minutes to hours, the typical temperature variation is about 0.1 K p-p. This kind of variation is so small that the temperature dependence of the quantum efficiency of the detector does not contribute to the noise (about a ppm rms!). Up to now the effect of the temperature has not been detected.

The instrument is also degrading due to the exposure to vacuum and to solar light. Figure 21 shows how the throughput has decreased over the past 8 years. It does not affect yet the noise performance of the instrument. Another minor problem has been detected in the VIRGO/SPM. The term coined is *attractor* as shown in Fig. 22 where it can be seen that the output of the instrument seems to be sometimes *attracted* to specific digital values. It does not occur very frequently for the LOI and contribute negligibly to the noise.

The major problem encountered is related to offpointing variations and/or temperature variations that are due to daily operations. These two effects introduce large offpointing inside the LOI of the order of tens of arcsec. Since the LOI operates in such a way that the axial symmetry is no kept (the secondary mirror being tilted), the occasional offpointing changes the light distribution at the focal plane of the detector. The inhomogeneous light distribution is due to aberrations that are not symmetrical around the normal of the primary mirror. This problem affects especially the guiding pixels that cannot yet be used for solar radius measurements.

The science performed with the LOI addresses three different subjects: p-mode seismology (Toutain et al., 1997; Appourchaux et al., 1998a,c; Gizon et al., 1998; Appourchaux, 1998; Appourchaux and Toutain, 1998; Fröhlich et al., 2001; Appourchaux, 2001; Appourchaux et al., 2002), g-mode detection (Fröhlich et al., 1998; Appourchaux et al., 2000,

† available at sohowww.nascom.nasa.gov/gallery/ESAPR/press33.html

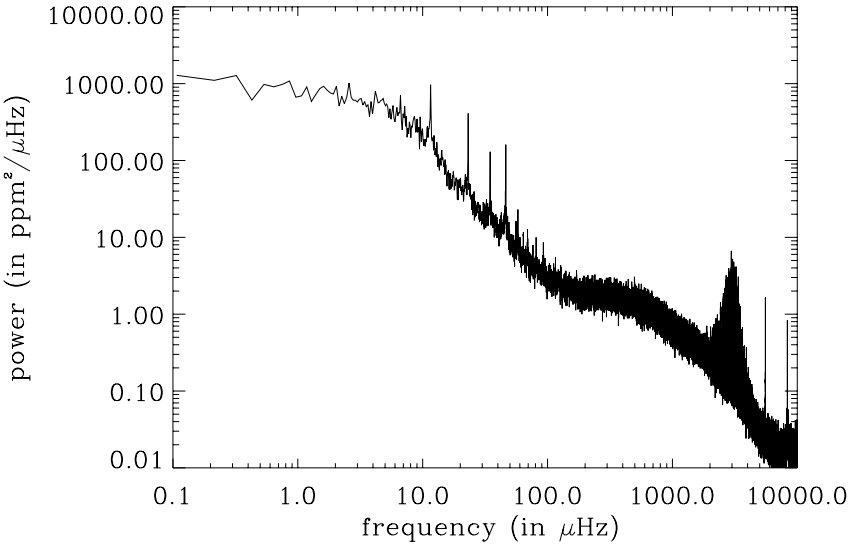

FIGURE 19. In-flight mean power spectrum of 26 times series of 108-day long each. The observation is about 7.7 years. The human interaction with the spacecraft manifests itself with the 24-hour frequency (11.57 μHz) and its first three aliases. The two large peaks at higher frequencies are due to the acquisition rate of the VIRGO instrument (3 minutes) and to the basic sampling of 1 minute. The p modes are easily seen at around 3 mHz, with an amplitude not larger than 8 ppm$^2/mu$Hz.

2001; Appourchaux, 2003) and helioseismic analysis (Appourchaux et al., 1998b,d). The latter is an interesting by-product that was not planned. It shows what can be achieved when instrumentation is only driven by Science.

5. Discussion and conclusion

The LOI exceeded its design performances. In retrospect, there are three design features that could have been better thought about.

The number of pixels is for instance rather limiting the capability of the instrument above $l = 3$ due to the mode aliasing. Doubling the number of pixels would have push the limit to $l = 4$ only. This would have severely made the electronics more complex by having 24 individual read out lines instead of 12. At least, we could have also put the guiding pixels on a read out using VFC...

Last but not least, it would have been better to have a separated coarse pointing that would have allowed to use to the telescope around its symmetry axis, and avoiding to have the secondary off pointed thereby destroying the symmetry of the telescope. At the time of design, a mechanism pointing the whole instrument towards the Sun required more space that was available for the whole LOI instrument. As far as the coarse pointing is concerned, this would require just a mere redefinition of the boundary conditions.

Since the end of 90's, the technology has evolved in such a way that it is now possible to have not only 24 pixels but about a million that can be read individually. These new detectors are called Active Pixel Sensors (APS). They are obviously the future for high photon flux application such as for the Sun or for star trackers imaging bright stars.

Unfortunately, from the scientific point of view, there would be very little sense to

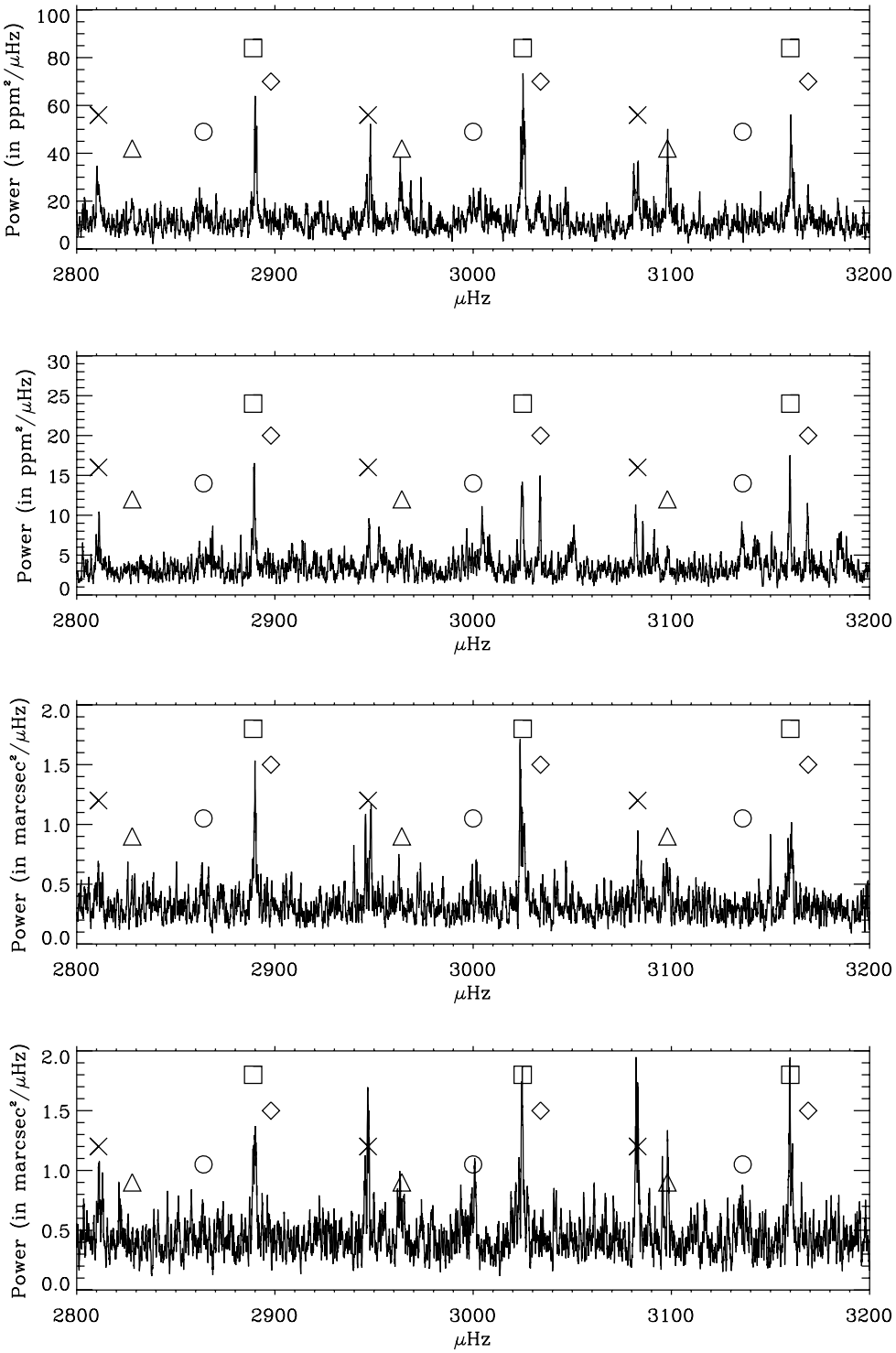

FIGURE 20. Power spectrum of the guiding pixels (two diagrams at the top) and of the high voltages (two diagrams at the bottom). The degree of the p-mode oscillation is indicated ($\diamond$ l=0, $\triangle$ l=1, $\square$ l=2, $\times$ l = 3, $\circ$ l=4). The frequency resolution is 54 nHz. The spectra are smoothed to 10 points to enhance the p-mode signals

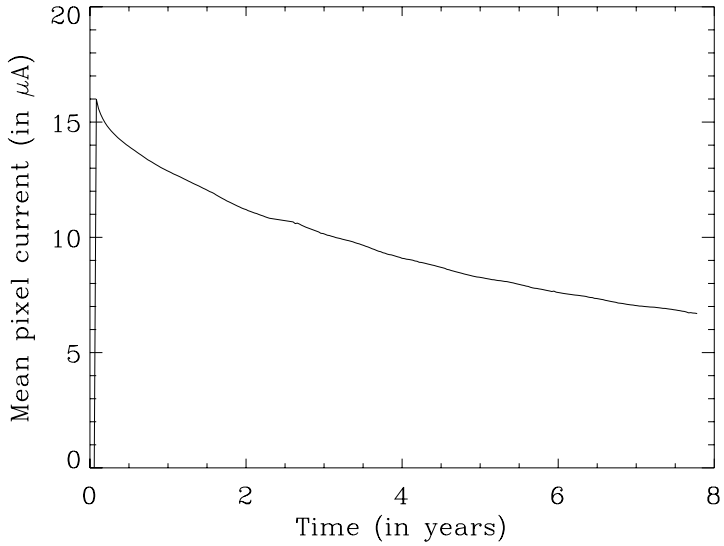

FIGURE 21. Variation of the current as provided by the pixels of the detector. The degradation shown here as an average over the 12 pixels affect them in the same manner. It is believed that the degradation is due to the detector and not to the entrance filter. The instrument can admit a reduction of throughput of a factor 8 before the electric noise becomes the limit.

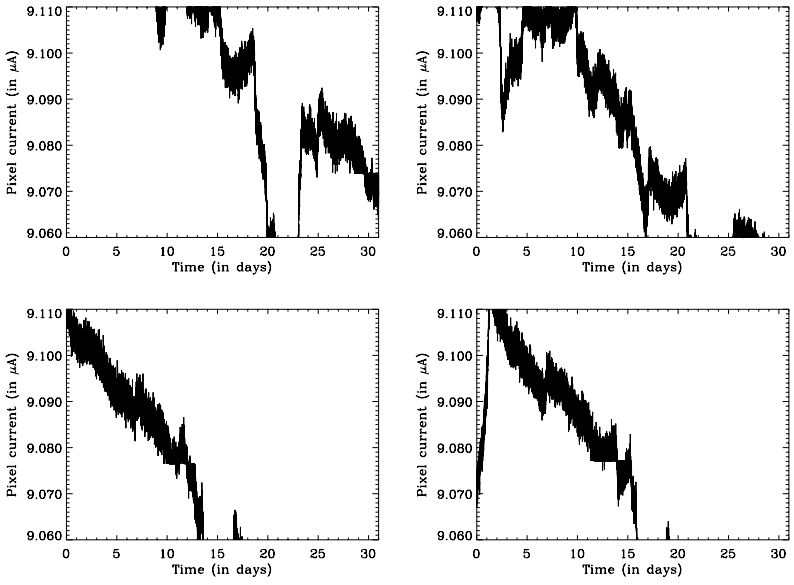

FIGURE 22. Signal measured by the four central pixels of the detector. On three of them, the *attractor* can easily be seen as locked value at around 9.75 μA. The attraction does not happen for each count but for some specific ones. This effect occurs also in the SPM. It is believed that it is due to the VFC locking onto these specific counts. The duration of the attractors is much shorter for the LOI than for the SPM because this latter does not degrade as fast as the LOI.

fly such a Next-Generation LOI...It would be very unlikely that we would be able to detect g modes with such an NG-LOI. In addition everything that could be learnt using p modes would be better done with an instrument detecting the modes in solar radial velocity†.

This state of affair shows that instrument building must be indeed driven by Science. Even though I found quite sad that I will not be able to build another LOI, and that this instrument is one of a kind, I have to accept the outcome of my own analysis. In due time I will find other ways of detecting g modes but they may not be based on such an instrument as the Luminosity Oscillations Imager (Appourchaux, 2003).

Acknowledgement. SOHO is a mission of international collaboration between ESA and NASA.

I am grateful to Trevor Sanderson of the Solar and Heliospheric Science Division of ESA. He was the one who proposed to replace the 'non-intelligence' of VIRGO by a well timed 'pulling of its plug'. We are also grateful to our colleagues of the Mechanics Section of ESTEC without whom my model of the cover could have not been validated: P.Coste, M.Eiden, M.York and M.Verin. Sincere thanks also to Matra-Marconi-Space (now Astrium, Toulouse) for the general management of the problem, to Saab for the implementation of the software patch and to P.Strada of the SOHO project for coordinating the software patch efforts. I am thankful to H.J.Roth for his faithful dedication to the VIRGO instrument and all tests performed on the spare.

The building of the LOI would have not been possible without the contribution of the following ESTEC personnel: J.Fleur, R.Scheper, A.Smit for the mechanical designs; J.Blommers, J.Postema, M.J.Kikkert, K.F.Frumau, for the machining and the assembling; K.Bouman, A.Fransen, J.Heida, L.Smit for the electronics fabrication; U.Telljohann, D.Martin, T.Beaufort for the electronic design; S.Lévêque for being *M*r Propre, for detector testing and for various optical tests and integration activities; additional contributions were given by G.Gourmelon for the spectrometry, by B.Johlander for various irradiations, by J.M.Guyt for checking the contamination, by A.Zwaal for the cleanliness levels and by P.Brault for the bakings; we also thank R.Czichy for loaning us the Zygo interferometer, and D.Doyle for the technical assistance for this interferometer. The various part of the LOI instrument could not have been built without the help of the following individuals: T.E.Hansen at Ame, C.Shannon and T.Hicks at Queensgate, and P.Robert at Bertin.

Last but not least the LOI would never have had a place in space without the efforts of the whole VIRGO team which are gratefully acknowledged. A special note to the dedication of Antonio Jiménez for operating the Virgo Data Center.

On a more personal note, I also thank my family for the unconditional support shown over the years. The family being my wife, Maryse, my two sons, Kevin and Thibault, and my two cats, Ah Kin and Myrtille. We succeeded.

References

Andersen, B., V. Domingo, A. Jones, A. Jiménez, P. Pallé, C. Régulo, and T. Roca Cortés: 1988. In: V.Domingo and E.Rolfe (eds.): *Seismology of the Sun and Sun-like Stars*. p. 385, ESA SP-286, ESA Publications Division, Noordwijk, The Netherlands.

† The signal-to-noise ratio in the power spectrum is about a factor 10 higher in velocity than in intensity. The lowest detectable frequency is about 1000 μHz in velocity, and 1800 μHz in intensity

Appourchaux, T.: 1998. In: S. Korzennik and A. Wilson (eds.): *Structure and Dynamics of the Interior of the Sun and Sun-like Stars*. p. 37, ESA SP-418, ESA Publications Division, Noordwijk, The Netherlands.

Appourchaux, T.: 2001. In: P.L.Pallé and A.Wilson (eds.): *Helio- and asteroseismology at the dawn of the millennium, SOHO-10/GONG 2000*. p. 71, ESA SP-464, ESA Publications Division, Noordwijk, The Netherlands.

Appourchaux, T.: 2003. In: H.Sawaya-Lacoste (ed.): *Proceedings of SOHO 12 / GONG+ 2002. Local and global helioseismology: the present and future*. p. 131, ESA SP-517, ESA Publications Division, The Netherlands.

Appourchaux, T., B. Andersen, G. Berthomieu, W. Chaplin, Y. Elsworth, W. Finsterle, C. Frölich, D. O. Gough, T. Hoeksema, G. Isaak, A. Kosovichev, J. Provost, P. Scherrer, T. Sekii, and T. Toutain: 2001. In: P.L.Pallé and A.Wilson (eds.): *Helio- and asteroseismology at the dawn of the millennium, SOHO-10/GONG 2000*. p. 467, ESA SP-464, ESA Publications Division, Noordwijk, The Netherlands.

Appourchaux, T., B. Andersen, C. Fröhlich, A. Jiménez, U. Telljohann, and C. Wehrli: 1997. *Solar Physics* **170**, 27.

Appourchaux, T., B. Andersen, and T. Sekii: 2002. In: C.Fröhlich and A.Wilson (eds.): *From Solar Min to Max: half a solar cycle with SOHO*. p. 47, ESA SP-508, ESA Publications Division, Noordwijk, The Netherlands.

Appourchaux, T. and B. N. Andersen: 1990. *Solar Physics* **128**, 91.

Appourchaux, T., W. J. Chaplin, Y. Elsworth, G. R. Isaak, C. P. MCLeod, B. A. Miller, and R. New: 1998a. In: F.-L. Deubner, J.Christensen-Dalsgaard, and D.Kurtz (eds.): *New eyes to see inside the sun and the stars, IAU 185*. p. 45, Kluwer Academic Publishers, Dordrecht, The Netherlands.

Appourchaux, T. and M. Cislaghi: 1992. *Optical Engineering* **31**, 1715.

Appourchaux, T., C. Fröhlich, B. Andersen, G. Berthomieu, W. Chaplin, Y. Elsworth, W. Finsterle, D. Gough, J. T. Hoeksema, G. Isaak, A. Kosovichev, J. Provost, P. Scherrer, T. Sekii, and T. Toutain: 2000. *ApJ* **538**, 401.

Appourchaux, T., L. Gizon, and M. C. Rabello-Soares: 1998b. *A&A Sup. Series* **132**, 107.

Appourchaux, T., M. C. Rabello Soares, and L. Gizon: 1998c. *IAU Symposia* **185**, 167.

Appourchaux, T., M.-C. Rabello-Soares, and L. Gizon: 1998d. *A&A Sup. Series* **132**, 121.

Appourchaux, T., U. Telljohann, D. Martin, J. Fleur, and S. Lévêque: 1995a. In: J. Hoeksema, V. Domingo, B. Fleck, and B. Battrick (eds.): *Helioseismology, 4th SOHO workshop*. p. 359, ESA SP-376, ESA Publications Division, Noordwijk, The Netherlands.

Appourchaux, T. and T. Toutain: 1998. In: J. Provost and F.-X. Schmider (eds.): *Sounding Solar and Stellar Interiors, IAU 181, Poster volume*. pp. 5+, Kluwer Academic Publishers, Dordrecht.

Appourchaux, T., T. Toutain, A. Jiménez, M. Rabello-Soares, B. Andersen, and A. Jones: 1995b. In: J. Hoeksema, V. Domingo, B. Fleck, and B. Battrick (eds.): *Helioseismology, 4th SOHO workshop*. p. 265, ESA SP-376, ESA Publications Division, Noordwijk, The Netherlands.

Appourchaux, T., T. Toutain, U. Telljohann, A. Jiménez, M. C. Rabello-Soares, B. N. Andersen, and A. R. Jones: 1995c. *A&A* **294**, L13.

Appourchaux, T. P.: 1993. *SPIE* **2018**, 80.

Appourchaux, T. P., G. Gourmelon, and B. Johlander: 1994. *Optical Engineering* **33**, 1659.

Appourchaux, T. P., D. D. Martin, and U. Telljohann: 1992. *SPIE* **1679**, 200.

Berthomieu, G. and J. Provost: 1990. *A&A* **227**, 563.

Bonnet, R. M., P. Lemaire, J. C. Vial, G. Artzner, P. Gouttebroze, A. Jouchoux, A. Vidal-Madjar, J. W. Leibacher, and A. Skumanich: 1978. *ApJ* **221**, 1032.

Chrétien, H.: 1958, *Calcul des combinaisons optiques*. Paris: Libr. du Bac, 1958/59, 4th ed.

Damé, L.: 1988. In: V.Domingo and E.Rolfe (eds.): *Seismology of the Sun and Sun-Like Stars*. p. 367, ESA SP-286, ESA Publications Division, Noordwijk, The Netherlands.

Delache, P. and P. H. Scherrer: 1983. *Nature* **306**, 651.

Fröhlich, C., B. Andersen, B. G., D. Crommelynck, P. Delache, V. Domingo, A. Jiménez, A. Jones, T. Roca Cortés, and C. Wehrli: 1988a. In: V.Domingo and E.Rolfe (eds.): *Seismology of the Sun and Sun-Like Stars*. p. 371, ESA SP-286, ESA Publications Division, Noordwijk, The Netherlands.

Fröhlich, C., T. Appourchaux, and D. Gough: 2001. In: P.L.Pallé and A.Wilson (eds.): *Helio- and asteroseismology at the dawn of the millennium, SOHO-10/GONG 2000*. p. 71, ESA SP-464, ESA Publications Division, Noordwijk, The Netherlands.

Fröhlich, C., R. M. Bonnet, A. V. Bruns, J. P. Delaboudinière, V. Domingo, V. A. Kotov, Z. Kollath, D. N. Rashkovsky, T. Toutain, and J. C. Vial: 1988b. In: V.Domingo and E.Rolfe (eds.): *Seismology of the Sun and Sun-Like Stars*. p. 359, ESA SP-286, ESA Publications Division, Noordwijk, The Netherlands.

Fröhlich, C., W. Finsterle, B. Andersen, T. Appourchaux, W. Chaplin, Y. Elsworth, D. Gough, J. T. Hoeksema, G. Isaak, A. Kosovichev, J. Provost, P. Scherrer, T. Sekii, and T. Toutain: 1998. In: S. Korzennik and A. Wilson (eds.): *Structure and Dynamics of the Interior of the Sun and Sun-like Stars*. p. 67, ESA SP-418, ESA Publications Division, Noordwijk, The Netherlands.

Fröhlich, C., J. Romero, H. Roth, C. Wehrli, B. N. Andersen, T. Appourchaux, V. Domingo, U. Telljohann, G. Berthomieu, P. Delache, J. Provost, T. Toutain, D. A. Crommelynck, A. Chevalier, A. Fichot, W. Däppen, D. Gough, T. Hoeksema, A. Jiménez, M. F. Gómez, J. M. Herreros, T. R. Cortés, A. R. Jones, J. M. Pap, and R. C. Willson: 1995. *Solar Physics* **162**, 101.

Gizon, L., T. Appourchaux, and D. O. Gough: 1998. In: F.-L. Deubner, J.Christensen-Dalsgaard, and D.Kurtz (eds.): *New eyes to see inside the sun and the stars, IAU 185*. p. 37, Kluwer Academic Publishers, Dordrecht, The Netherlands.

MacLeod, H. A.: 1986, *Thin-Film Optical Filters*. Institute of Physics Publishing, London, UK.

Marco, J., A. Chourreau, and H. Oscar: 1994, "Essai de longue durée sur revêtements de régulation thermique', CERT 439700'. Technical report, Centre d'étude de recherches de Toulouse, France.

Rabello-Soares, M. C., T. Roca Cortès, A. Jiménez, B. N. Andersen, and T. Appourchaux: 1997a. *A&A* **318**, 970.

Rabello-Soares, M. C., T. Roca Cortès, A. Jiménez, T. Appourchaux, and A. Eff-Darwich: 1997b. *ApJ* **480**, 840.

Scherrer, P., J. Hoeksema, R. Bogard, and et al: 1988. In: V.Domingo and E.Rolfe (eds.): *Seismology of the Sun and Sun-Like Stars*. p. 367, ESA SP-286, ESA Publications Division, Noordwijk, The Netherlands.

Toutain, T., T. Appourchaux, F. Baudin, C. Froehlich, A. Gabriel, P. Scherrer, B. N. Andersen, R. Bogart, R. Bush, W. Finsterle, R. A. Garcia, G. Grec, C. J. Henney, J. T. Hoeksema, A. Jimenez, A. Kosovichev, T. R. Cortes, S. Turck-Chieze, R. Ulrich, and C. Wehrli: 1997. *Solar Physics* **175**, 311.

van der Raay, H. B.: 1988. In: V.Domingo and E.Rolfe (eds.): *Seismology of the Sun and Sun-Like Stars*. p. 339, ESA SP-286, ESA Publications Division, Noordwijk, The

Netherlands.
Woodard, M.: 1984, "Short-period oscillations in the total solar irradiance". Ph.D. thesis, University of California, San Diego.